

CONFIDENTIAL

**NASA TECHNICAL
MEMORANDUM**



OR
NASA TM X-1366

REFERENCE

NOV 09 2004

**COMPONENT FLOW AND
FLUID PROPERTIES DURING
COLD-FLOW EXPERIMENTS IN
A NUCLEAR ROCKET SYSTEM**

CLASSIFICATION CHANGED
To Unclassified
By authority of H. A. Mainis
Date Jan 3, 1973
per lmd

*by David M. Straight, Thomas J. Biesiadny,
John G. Pierce, and George W. Metger*

*Lewis Research Center
Cleveland, Ohio*

LIBRARY COPY

MAY 16 1967

LEWIS LIBRARY, NASA
CLEVELAND, OHIO

COMPONENT FLOW AND FLUID PROPERTIES DURING COLD-FLOW
EXPERIMENTS IN A NUCLEAR ROCKET SYSTEM

By David M. Straight, Thomas J. Biesiadny,
John G. Pierce, and George W. Metger

Lewis Research Center
Cleveland, Ohio

RESTRICTED DATA

ATOMIC ENERGY ACT OF 1954

GROUP 1

Excluded from automatic
downgrading and declassification

CLASSIFIED DOCUMENT-TITLE UNCLASSIFIED

This material contains information affecting the national defense of the United States within the meaning of the espionage laws, Title 18, U.S.C., Secs. 793 and 794, the transmission or revelation of which in any manner to an unauthorized person is prohibited by law.

NOTICE

This document should not be returned after it has satisfied your requirements. It may be disposed of in accordance with your local security regulations or the appropriate provisions of the Industrial Security Manual for Safe-Guarding Classified Information.

NATIONAL AERONAUTICS AND SPACE ADMINISTRATION

~~CONFIDENTIAL~~

COMPONENT FLOW AND FLUID PROPERTIES DURING COLD-FLOW EXPERIMENTS IN A NUCLEAR ROCKET SYSTEM (U)

by David M. Straight, Thomas J. Biesiadny,
John G. Pierce, and George W. Metger

Lewis Research Center

SUMMARY

The experimental heat-transfer and flow data obtained in several different startup chilldown transients were analyzed to determine the time history of flow rate, fluid properties, and accumulation of hydrogen in the various components of a full-scale simulated nuclear rocket system. As much as 70 percent of the flow entering the system in the first 3 seconds was stored in the system; the storage was greater at low tank pressures. The time and space history of two-phase flow was followed through the system. A detailed analysis for a selected run showed that two-phase flow prevailed for about 4 seconds at stations upstream of the reflector and existed over about 20 feet of the length of the system early in the run. Large flow, density, and enthalpy gradients existed in time and space.

An interpolation solution between the flow entering and leaving the system was used to calculate the flow rates at various intermediate stations. This approach, although approximate, produced calculated results that were in reasonable agreement with experimental values at one intermediate station in the system.

INTRODUCTION

The determination of flow rate and fluid properties at various stations in an engine system during the initial chilldown phase has long been a problem in the design of engine systems that employ cryogenic fluids. In chemical rockets, for example, the startup transient usually occurs in a very short time. Continuous control of engine variables during the startup is usually not possible because determination of the propellant fluid properties and flow rates during the rapid transient is difficult. In the nuclear rocket, the problem is of greater significance because the startup transient is of longer duration

~~CONFIDENTIAL~~

CONFIDENTIAL

and continuous control is not only possible but essential for safe operation. Development of a control system for the nuclear rocket requires that the hydrogen flow rate and fluid property changes resulting from heat transfer are known.

It is during chilldown that two-phase flow occurs with its associated problems of heat transfer and flow storage (liquid accumulation) in the components of the system. In addition, dynamic flow oscillations and interactions occur that are not well understood.

Flow-rate and fluid-property information is required for heat-transfer analyses of the components such as the feedline, nozzle (ref. 1), reflector and core (ref. 2). Component analyses result in calculated temperature rise, pressure drop, and material temperature gradients required for thermal-stress analyses. The component analyses are also important for determining bootstrap capability (using the latent heat of the components) during startup, that is, whether enough energy is available at the turbine to pump sufficient liquid hydrogen until reactor power is available. In addition, the flow-rate and fluid-property information is required base-line information for the study of flow dynamics in the system that, in turn, affects the dynamic behavior of the controls for the system.

A method for calculating the cooldown time of cryogenic transfer lines is presented in reference 3. No attempt was made, however, to calculate the time history of flow rate and fluid properties at various stations during the transition from gas to liquid as the system cooled down. Ideally, it is desirable to be able to calculate, without expensive experimental input data, the flow rate and fluid properties throughout a system with only an assumed supply pressure or inlet flow rate and the initial temperature of the components. Reference 4 reports such a calculation procedure for predicting heat transfer and flow in a complete nuclear rocket system. For accurate results when such procedures are used, however, it is necessary that adequate heat-transfer and pressure-drop laws be available for all the heat-transfer regimes encountered. During chilldown, for example, the heat-transfer regimes encountered include the flow of heat into a liquid, a two-phase mixture, and a gas. The present knowledge of heat transfer is meager in the transition regions between these heat-transfer regimes and between two-phase nucleate and film boiling (refs. 5 to 7).

This report presents the heat-transfer analysis of data obtained in a full-scale nuclear-rocket-system experiment conducted at the Lewis Research Center, Plum Brook Station. The system is close coupled and has a thermal heat capacity that simulates a typical flight installation. Data from selected runs were analyzed to determine the time history of flow rate, density, temperature, and enthalpy of the fluid at various stations in the system.

The equations used in the data analysis were derived from the continuity and energy equations. Assumptions and simplifications were incorporated to permit more rapid processing of the data for engineering purposes. Maximum use was made of available experimental data. The heat transfer, for example, from the components to the fluid

CONFIDENTIAL

was obtained from the experimental temperature-time history of the components instead of calculations based on heat-transfer laws. The flow rates entering and leaving the system were also available from experimental measurements.

No attempt is made in this report to describe the complete dynamic behavior of two-phase flow or to predict the flow and heat transfer in the system knowing only the initial input conditions. The reader is referred to reference 8 for a more rigorous treatment of this problem of two-phase flow dynamics during chilldown and the difficulties encountered in the numerical analysis.

Quasi-steady-state results are presented at four major stations for three runs where different supply pressures were used and at 13 stations for another run where a maximum startup flow-rate ramp was used. Problem areas are discussed, and accuracies evaluated by comparing calculated fluid properties with experimental values were available.

ANALYSIS

Derivations and Approximations

In fluid dynamics (ref. 9, e.g.) for the special case of one-dimensional frictionless compressible flow in a constant cross-sectional area tube, the dynamic flow equations may be written as follows (the symbols are defined in appendix A):

Continuity:

$$A \frac{\partial \rho}{\partial t} + \frac{\partial}{\partial x} (\rho A v) = 0 \quad (1)$$

Momentum (no gravity):

$$A \frac{\partial}{\partial t} (\rho v) + \frac{\partial}{\partial x} (\rho A v^2) + A \frac{\partial p}{\partial x} = 0 \quad (2)$$

Energy (no heat flow, no gravity):

$$A \frac{\partial}{\partial t} \left[\rho \left(u + \frac{1}{2} v^2 \right) \right] + \frac{\partial}{\partial x} \left[\rho A v \left(h + \frac{1}{2} v^2 \right) \right] = 0 \quad (3)$$

Equations were derived from these basic equations by using a number of engineering approximations that enabled calculation of the enthalpy, density, and flow rate of the fluid at any desired station in the system using experimental heat flow rates and pressure.

[REDACTED]

Since experimental pressures were available, the momentum equation (eq. (2)) was not used in the derivation. Additionally, the extreme sensitivity of flow rate to small pressure changes made use of the momentum equation undesirable for calculation of flow rate.

The kinetic energy term $1/2 v^2$ in equation (3) was small compared with the internal energy u for the range of flow conditions encountered in the experiment. This term was therefore deleted and the heat flow rate term added as follows:

$$A \frac{\partial}{\partial t} (\rho u) + \frac{\partial}{\partial x} (\rho A v h) = \frac{\partial \dot{Q}_m}{\partial x} \quad (4)$$

where \dot{Q}_m is the heat flow rate from the material of the components determined from experimental measurements. Since $u = h - (p/\rho)$ and $\rho A v = \dot{w}$, equation (4) may be written as

$$A \frac{\partial}{\partial t} \left[\rho \left(h - \frac{p}{\rho} \right) \right] + \frac{\partial}{\partial x} (\dot{w} h) = \frac{\partial \dot{Q}_m}{\partial x}$$

or

$$A \frac{\partial}{\partial t} (\rho h) - A \frac{\partial p}{\partial t} + \frac{\partial}{\partial x} (\dot{w} h) = \frac{\partial \dot{Q}_m}{\partial x} \quad (5)$$

The pressure term $A(\partial p/\partial t)$ was also small relative to the other terms and was deleted:

$$A \frac{\partial}{\partial t} (\rho h) + \frac{\partial}{\partial x} (\dot{w} h) = \frac{\partial \dot{Q}_m}{\partial x} \quad (6)$$

The continuity equation (eq. (1)) may be written as

$$A \frac{\partial \rho}{\partial t} + \frac{\partial \dot{w}}{\partial x} = 0 \quad (7)$$

Experimental input data were available at finite time and space (length) intervals. Equations (6) and (7) were therefore transformed into difference equations and combined so that the experimental data may be used directly and then solved for the enthalpy at the outlet station of an incremental length. From the calculated value of enthalpy and the corresponding experimental static pressure at the station, a value for density was determined from hydrogen property data.

~~CONFIDENTIAL~~

Problems of stability and/or accumulative errors (ref. 8), however, became apparent in the solution for flow rate (eq. (7)) throughout the system by using only the inlet flow rate and experimental pressure and heat flow rates. Instead of using equation (7), a direct interpolation technique between flow rate entering and leaving the system was adopted, which is discussed in the section Calculation Procedure.

A typical solution for the enthalpy at the outlet of an incremental length Δx , using finite differences, may be written as follows:

$$h(x, t) = h(x - \Delta x, t) + \frac{\dot{Q}_m(x, t) - \dot{Q}_m(x - \Delta x, t)}{\dot{w}(x, t)} + \frac{A \Delta x}{\Delta t \dot{w}(x, t)} \left\{ h(x - \Delta x, t) [\rho(x, t) - \rho(x, t - \Delta t)] - [\rho(x, t)h(x, t)] + [\rho(x, t - \Delta t)h(x, t - \Delta t)] \right\} \quad (8)$$

An iterative solution is required since the density $\rho(x, t)$ is a function of $h(x, t)$ being calculated. In this case, however, the numerical values of the third term on the right side of equation (8) (which includes the stored energy terms) were small relative to the other terms after the first 2 seconds of run time. (The first 2 sec of a run include the initial surge of liquid into the system and flow oscillations.) Equation (8) then reduces to

$$h(x, t) = h(x - \Delta x, t) + \frac{\dot{Q}_m(x, t) - \dot{Q}_m(x - \Delta x, t)}{\dot{w}(x, t)} \quad (9)$$

The system being analyzed was divided into a number of incremental lengths. Equation (9) may then be written by using a system notation as follows:

$$h_j = h_D + \sum_D^j \frac{\dot{Q}_{m,i}}{\dot{w}_{out}} \quad (10)$$

where station D is the inlet station of the system, j is any other station in the system, and i is the length increment between adjacent stations. Also, since the system outlet conditions (\dot{w}_P , h_P) are known, equation (9) may be rearranged as follows:

$$h_j = h_P - \sum_j^P \frac{\dot{Q}_{m,i}}{\dot{w}_{in}} \quad (11)$$

~~CONFIDENTIAL~~

CONFIDENTIAL

In equation (10), the solution for enthalpy at any station in the system is determined by working forward (downstream) from the system inlet. Conversely, equation (11) may be used to obtain the enthalpy at that same station by working backward (upstream) from the system outlet.

It was desired to obtain \dot{w} , h , and ρ at particular stations located near the center of the system without having to solve for flow rates at each of the intervening stations in the system. For these calculations, equation (10) (forward solution) and equation (11) (backward solution) were written as follows:

$$h_j = h_D + \frac{\sum_{i=1}^j \dot{Q}_{m,i}}{\dot{w}_{out,j}} \quad (12)$$

$$h_j = h_P - \frac{\sum_{i=j}^P \dot{Q}_{m,i}}{\dot{w}_{in,j}} \quad (13)$$

Although both these equations divide the system into two large volumes, comparisons between results from equation (12) or (13) agreed with the results from the corresponding equation (10) or (11) within the accuracy of the input data.

Calculation Procedure

A schematic diagram of the complete research apparatus is shown in figure 1. The calculation procedure required that the system be divided into a series of incremental lengths. These sections are shown schematically in figures 1 and 2, where the outlet from each incremental length is identified by the station symbols A, B, etc. Station D is located at the inlet to the main valve, the inlet to the first incremental length. The system upstream of the main valve (fig. 1) was precooled and full of liquid hydrogen. The heat transfer in this section was assumed to be equal to zero in the analysis. The materials, weight, internal fluid volume, and flow area of each incremental length are presented in table I.

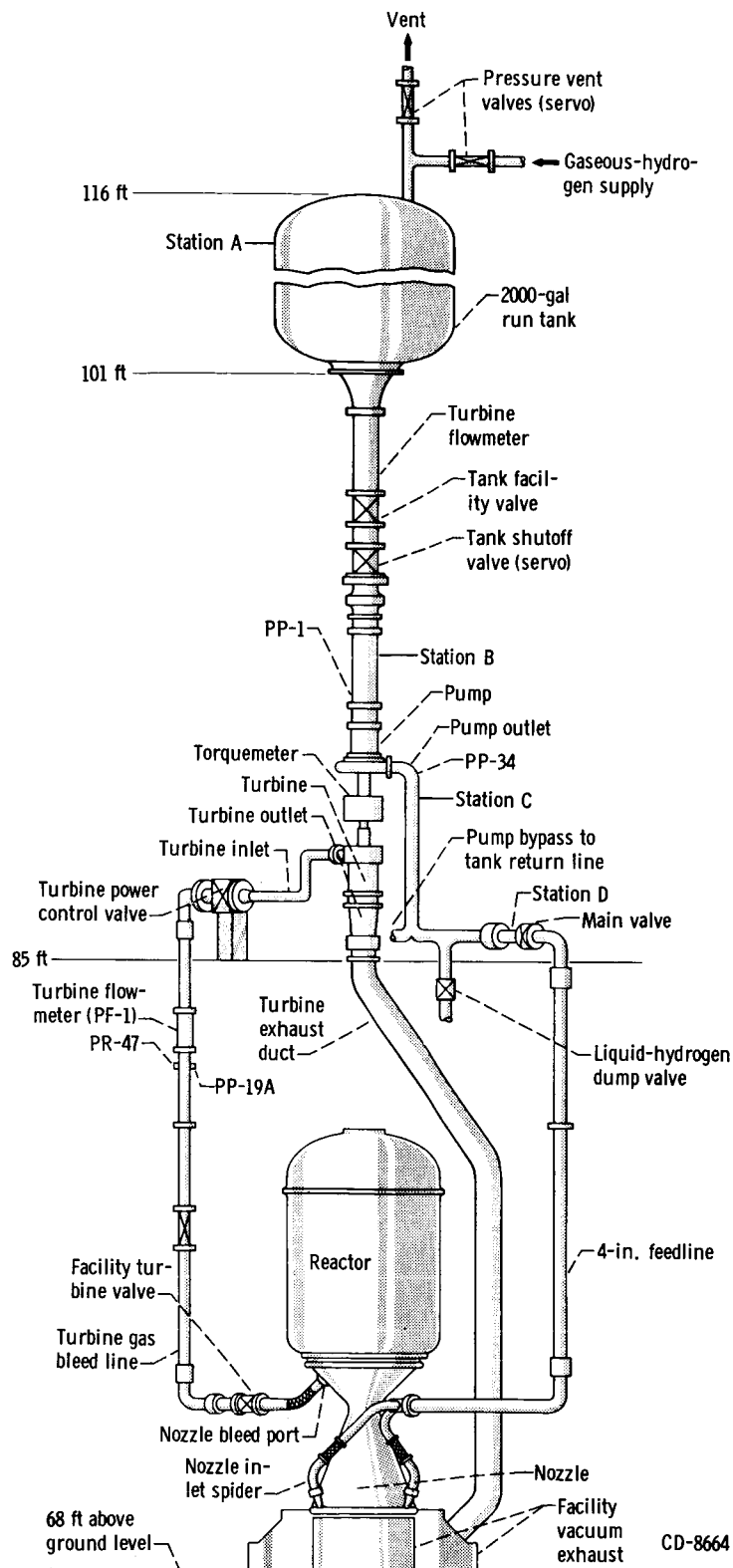


Figure 1. - Schematic diagram of nuclear-rocket cold-flow system.

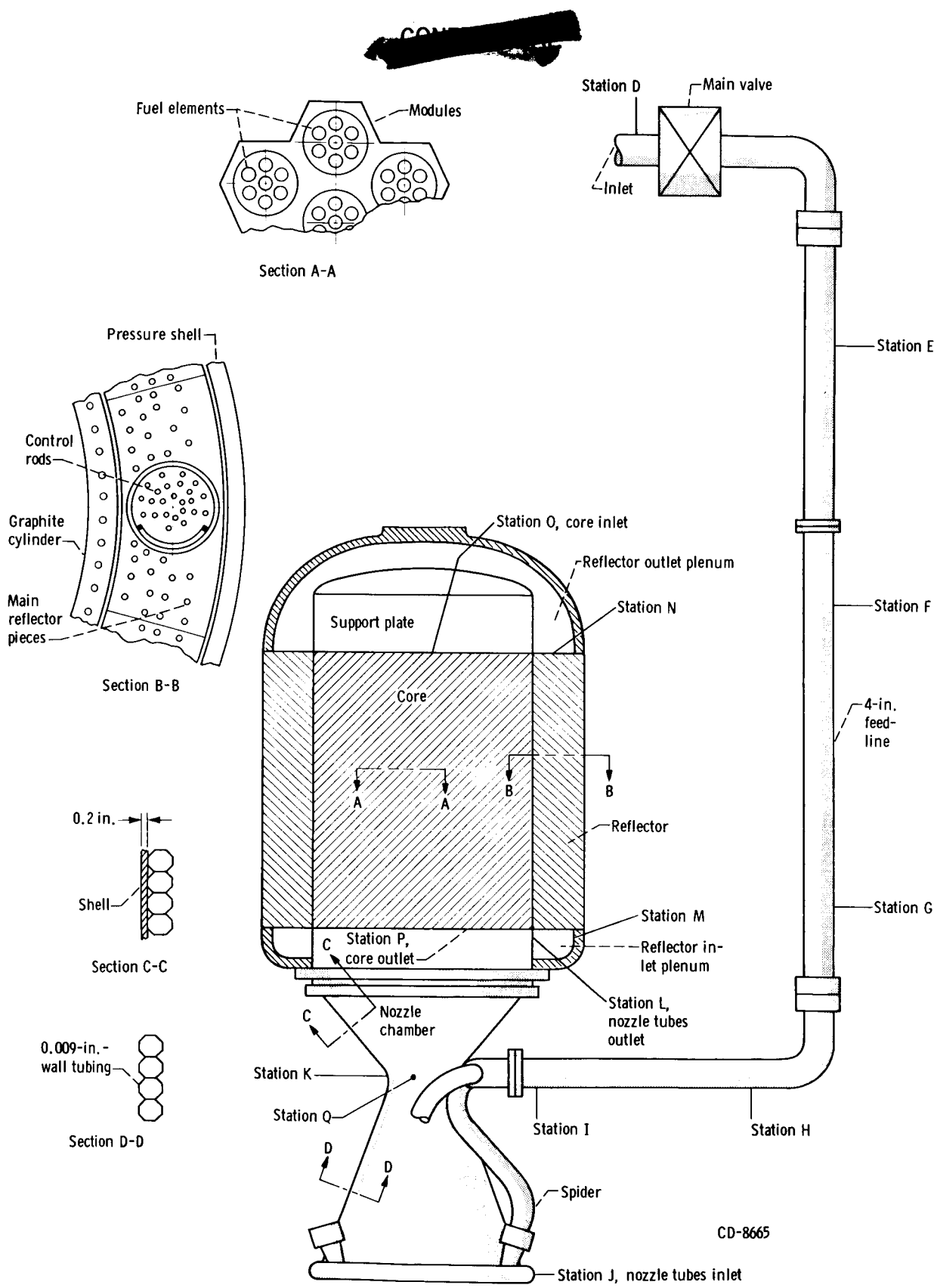


Figure 2. - Schematic diagram of incremental lengths used in heat-transfer analysis.

TABLE I. - GEOMETRY OF HEAT-TRANSFER INCREMENTS

Description	Station	Material	Weight, ^a $\rho_m V_m$, lb	Fluid volume, cu ft	Flow area, sq ft
Propellant feedline:	D to E	304 Stainless steel	12	0.32	0.10
	E to F	↓	15	.38	↓
	F to G		16	.41	
	G to H		12	.31	
	H to I		14	.38	↓
Spider and manifold	I to J	↓	90	.66	.09
Nozzle:					
Coolant tubes	J to K	Inconel X	42	0.51	0.322 to 0.048
Coolant tubes	K to L	Inconel X	32	.65	0.048 to 0.463
Nozzle shell	K to L	Inconel X	192	----	-----
Reflector inlet plenum	L to M	Aluminum	360	1.53	----
Reflector:					
Pressure shell	M to N	Aluminum	1000	1.98	0.43
Main reflector	M to N	Aluminum	2470	↓	↓
Control rods	M to N	Aluminum	610	↓	↓
Graphite cylinder	M to N	Graphite	732	↓	↓
Dome:					
Pressure shell	N to O	Aluminum	418	7.48	----
Support plate	N to O	Aluminum	289	7.48	----
Core:					
Modules and fuel elements	O to P	Graphite	2700	5.08	1.04
Nozzle chamber	P to Q	-----	----	9.17	7.23 to 0.415

^aWeight assigned for heat-transfer purposes; external nuts, bolts, clamps, etc., not included.

Experimental inputs. - The heat transferred to the hydrogen from the component parts \dot{Q}_m in equations (12) and (13) was calculated from the time history of thermocouple data as follows:

$$\dot{Q}_{m,i} = \frac{(\rho_m V_m) \int_{T_{m,t}}^{T_{m,t-\Delta t}} C_p(T_{m,i}) dT_{m,i}}{\Delta t} \quad (14)$$

The time interval Δt was the printout interval (0.336 sec) of the data.

~~CONFIDENTIAL~~

The values of \dot{Q}_m for the system incremental lengths were usually the sums of several smaller lengths within the increment shown in figure 2. For example, a material temperature measurement was taken at about every 12 inches on the propellant feedline (increment lengths in the feedline were about 40 in.). The values for \dot{Q}_m in the larger components, such as the nozzle, reflector, and core, were sums of the \dot{Q}_m values of the component parts of the assembly (such as sections A-A and B-B, fig. 2) so that proper weighting was accomplished.

Equation (14) does not account for transient conduction effects in the components. In the 4-inch feedline, for example, measurements were made on the outside of the pipe wall, and the heat transferred to the hydrogen during the time the thermal gradient was being established in the wall thickness was greater than that indicated by the measurement. This error, however, was significant only in the first second of cooldown (calculation method of ref. 10). Transient conduction error was insignificant in the large components farther downstream because the measurements were made within the material, and the rate of change of thermal gradients was also much slower.

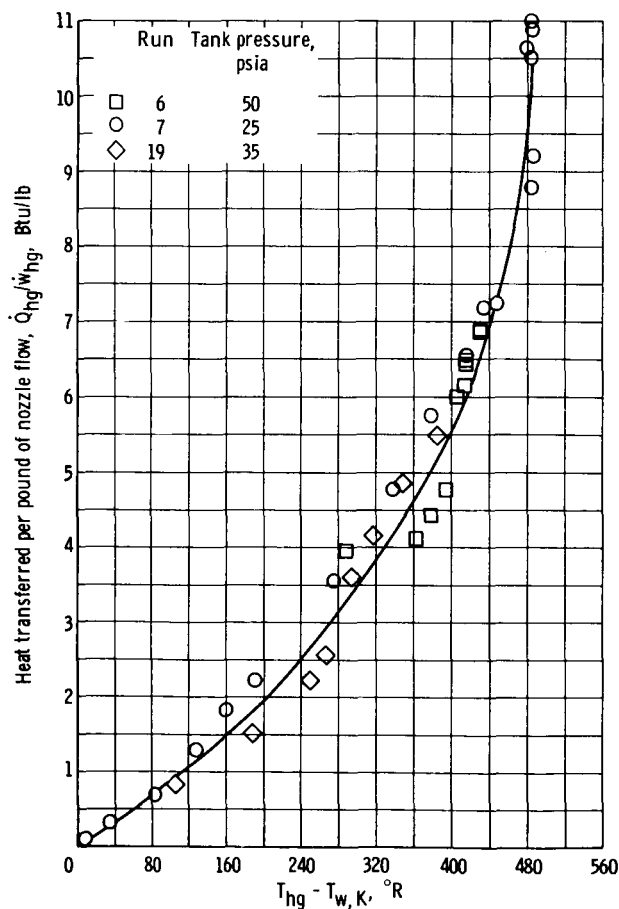


Figure 3. - Calculated heat transfer in whole nozzle from hot-gas side fluid to nozzle tube walls during cooldown transients.

The heat transferred from the warmer gas on the exhaust side of the nozzle coolant tubes through the wall to the coolant-side fluid was not included in the calculations. In order to obtain some estimate of this heat transfer, sample calculations were made for three selected runs, runs 6, 7, and 19, at different flow rates (tank pressures of 50, 25, and 35 psia, respectively). For these runs, $\dot{Q}_{hg}/\dot{w}_{hg}$ as a function of ΔT was determined as follows: ΔT was taken as the difference between core exit fluid temperature and nozzle throat material temperature, \dot{w}_{hg} was taken as the nozzle throat exhaust flow rate \dot{w}_Q , and \dot{Q}_{hg} was calculated by the method of reference 1. Results of the calculations are plotted in figure 3 and were in sufficiently close agreement to permit generalization by constructing a mean curve through the data.

Figure 3 was useful for estimating the total hot-gas-side heat transfer in the nozzle during chilldown runs, where the

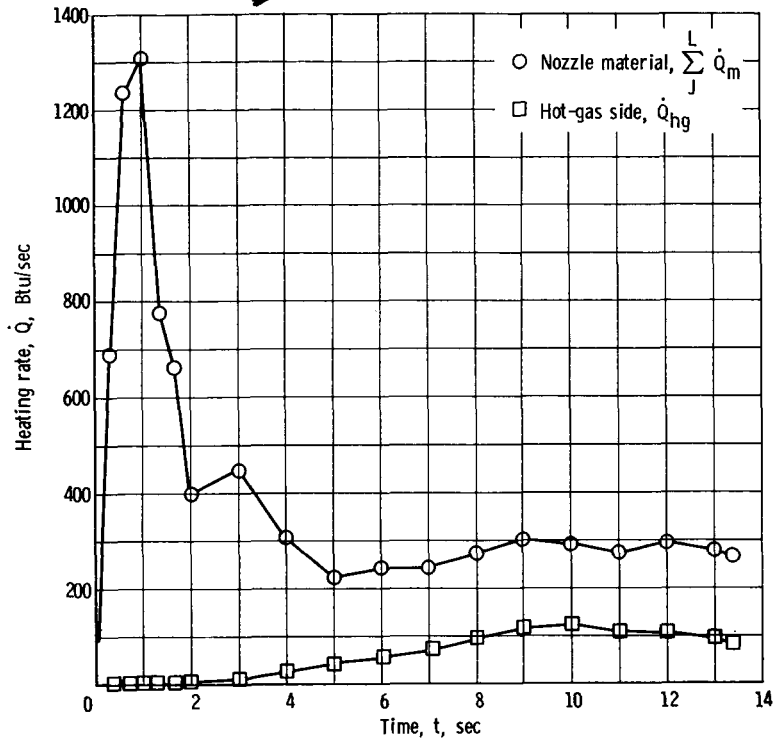


Figure 4. - Comparison of rate of heat transfer from nozzle hot-gas side to heat loss from nozzle material. Run 24.

detailed information obtained by the method of reference 1 was not necessary. A comparison of estimated \dot{Q}_{hg} (fig. 3) with \dot{Q}_m (eq. (14)) for run 24 is presented in figure 4. Compared with \dot{Q}_m , \dot{Q}_{hg} is of major significance after 4 seconds in the run illustrated. Even though it is important for the nozzle as a component, both \dot{Q}_m (after 4 sec) and \dot{Q}_{hg} (for the whole run) are insignificant compared with the total heat transfer in the whole system (about 20 000 Btu/sec at 7 sec).

No allowance was made for heat transfer from the ambient surroundings to the component parts. The feedline and nozzle were insulated to reduce this heat leak. The heat capacity of the insulation was also not included in the determination of the heat flow rates.

The flow rate entering the system was a direct measurement. The flow rate leaving the system, however, was determined from average temperature and pressure measurements in the exhaust nozzle chamber and the following equations. For choked isentropic flow at the at the nozzle throat,

$$p_Q = p_P \left(\frac{2}{\gamma + 1} \right)^{\gamma/(\gamma-1)} \quad (15)$$

the flow rate was

$$\dot{w}_Q = 40.08 C_D \Phi \sqrt{\rho(p_P - p_Q)} \quad (16)$$

where the expansion factor

$$\Phi = \sqrt{\frac{0.9965 \left(\frac{\gamma}{\gamma - 1} \right) \left(\frac{p_Q}{p_P} \right)^{2/\gamma} \left[1 - \left(\frac{p_Q}{p_P} \right)^{(\gamma-1)/\gamma} \right]}{\left[1 - 0.0035 \left(\frac{p_Q}{p_P} \right)^{2/\gamma} \right] \left[1 - \left(\frac{p_Q}{p_P} \right) \right]}}$$

The flow coefficient C_D was assumed to be equal to 1. To obtain the total flow leaving the system (at station P), the turbine flow leaving the system through the nozzle bleed port (fig. 1, p. 7) was added to the nozzle flow rate \dot{w}_Q .

In addition to the static pressure measurements at each station, the enthalpies of the fluid entering and leaving the system was required. The enthalpies were determined from the experimental fluid temperatures, pressures and hydrogen properties.

Interpolation solution. - The calculation proceeded by first solving for the enthalpy of the fluid as a function of time at a selected station to determine when liquid hydrogen first arrived (start of two-phase flow) and when subcooled liquid first arrived (end of two-phase flow) at that station. The assumption was made that $\dot{w}_{out,j}$ in equation (12) (or $\dot{w}_{in,j}$ in eq. (13)) was equal to \dot{w}_P , the flow rate leaving the last increment in the system. The enthalpy h_j was then calculated at several times from $t = 0$ to the time when the calculated h_j was equal to h_{sg} , the enthalpy of saturated vapor corresponding to the static pressure at the station. When $h_j = h_{sg}$, two-phase flow (and flow storage) began.

Large errors in values of the calculated enthalpy at a station resulted if the forward solution (eq. (12)) was used near the system outlet or if the backward solution (eq. (13)) was used near the system inlet. This was the result of cumulative errors in the measured heat-flow rates (± 10 percent) and the sensitivity of h_j to \dot{Q}_m/\dot{w}_j . These errors were minimized by using equation (12) when $\sum_D^j \dot{Q}_{m,i}$ was less than $\sum_P^j \dot{Q}_{m,i}$ and by using equation (13) when $\sum_j^P \dot{Q}_{m,i}$ was less than $\sum_D^j \dot{Q}_{m,i}$.

The flow-rate assumption used for the interpolation solution states that, when only the gaseous state exists downstream of the station, no flow storage exists beyond the station; that is, from the station being analyzed to the exhaust nozzle, and during the

time from $t = 0$ to time when $h_j = h_{sg}$, the system downstream of the station was full of gaseous hydrogen. Although the density of the gas in this part of the system changed by as much as a factor of 100 as a result of pressure and temperature changes, the change in mass of gas in this portion of the system was small (less than 5 percent) compared with the mass stored in the portions of the system having two-phase flow.

The start of subcooled liquid flow (end of two-phase flow) at a station was determined by first assuming that $\dot{w}_{out,j}$ in equation (12) (where $\sum_D \dot{Q}_{m,i}$ was always $< \sum_j \dot{Q}_{m,i}$) was equal to \dot{w}_D (assumed to be equal to \dot{w}_f) the flow entering the system. The enthalpy h_j was calculated at several times starting with the time at the end of the run and proceeding toward the beginning of the run until h_j equalled h_{sl} , the enthalpy of saturated liquid, corresponding to the static pressure at the station being analyzed. The time when $h_j = h_{sl}$ was taken as the end of two-phase flow (and the end of flow storage). The assumption of using \dot{w}_D for $\dot{w}_{out,j}$ in equation (12) states that when subcooled liquid was present, no flow storage existed; that is, the portion of the system between the inlet and the station being analyzed was completely full of liquid after the time when $h_j = h_{sl}$. The change in mass of liquid hydrogen due to pressure and temperature changes was negligible compared with mass storage occurring in two-phase flow portions of the system.

The variation of fluid enthalpy with time at a station was then plotted for the gas phase and the liquid phase, as shown in figure 5. After the time boundaries were established for the two-phase flow interval (fig. 5), a flow-rate curve for this station had to be established. During the two-phase flow interval, large changes in fluid density occurred at the station; consequently, neither the system inlet flow-rate values nor the system outlet values applied, and some intermediate values had to be obtained. For this purpose, the time scale $t_{sl} - t_{sg}$ was divided into a number of intermediate time increments, and the value of flow rate \dot{w}_{int} at each intermediate time was assumed to vary as follows

$$\dot{w}_{int} = \dot{w}_P + \frac{t_{int} - t_{sg}}{t_{sl} - t_{sg}} (\dot{w}_D - \dot{w}_P) \quad (17)$$

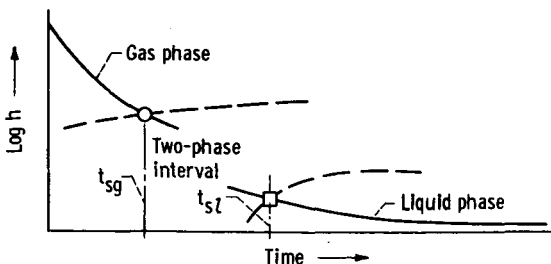


Figure 5. - Typical variation of enthalpy with time.

where t_{int} identifies the particular time being considered. A curve joining these interpolated values of \dot{w}_{int} yielded the estimated flow rate during two-phase flow for use in the analyses.

The resulting flow rate curve is illustrated in figure 6. The interpolated values of flow rate \dot{w}_{int} were then used in equation (12) to

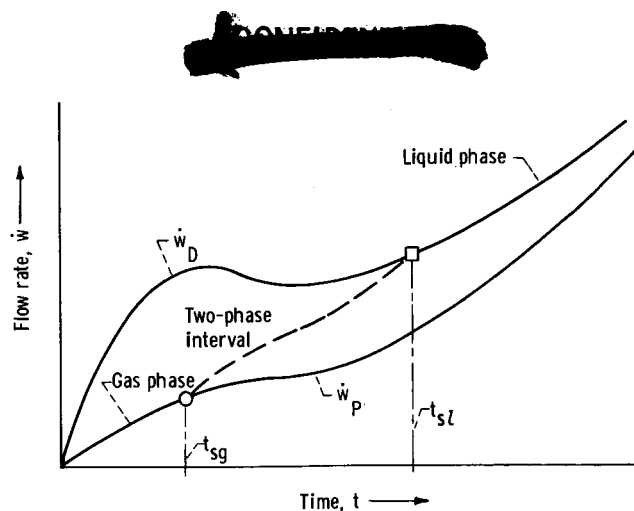


Figure 6. - Typical variation of flow rate with time.

obtain values of enthalpy at a station during the two-phase interval with the assumption that saturation equilibrium conditions prevailed.

Stations N, O, and P in some runs remained in the gas phase for the duration of the run. In these cases, \dot{w}_P was used for the complete run. Equation (12) or (13) was used, the choice being determined by the accuracy criteria.

Mass balance. - A check on the accuracy of the calculation procedure and the experimental data was made by comparing the total mass of hydrogen stored in the system, determined from the calculations, with the difference in total mass that entered and left the system, determined from experimental measurements. Thus, at time t , the following equation should be true

$$\sum_D^Q M_{st,i} = \int_0^t \dot{w}_D dt - \int_0^t \dot{w}_P dt \quad (18)$$

where

$$M_{st,i} = \bar{\rho}_i V_i \quad (19)$$

and

$$\bar{\rho}_i \sim \frac{\rho_{in,i} + \rho_{out,i}}{2} \quad (20)$$

Equation (20) is only approximate since the actual density gradient was nonlinear in the increment.

Heat balance. - A check on the accuracy of the experimental data was made by comparing the total heat flow rate (heat loss) from the components with the heat flow-rate increase in the hydrogen as it passed through the system

$$\dot{Q}_{fl, P} - \dot{Q}_{fl, D} = \sum_D^P \dot{Q}_{m, i} \quad (21)$$

for the assumption that there was no heat transfer between stations P and Q. The fluid heat flow rates are

$$\dot{Q}_{fl, w} = \dot{w}_P h_P$$

and

$$\dot{Q}_{fl, D} = \dot{w}_D h_D$$

Evaluating the right and left sides of equation (21) requires a correction for the time it takes a parcel of fluid to pass through the system. For this correction, it was necessary to use some of the output of the calculated results.

The transit time t_t was calculated as a function of time at station D for each volume increment by using the following equation

$$t_{t, i} = \frac{\bar{\rho}_i}{\dot{w}_i} V_i \quad (22)$$

where

$$\bar{\rho} = \frac{\rho_{in, i} + \rho_{out, i}}{2}$$

and

$$\bar{\dot{w}}_i = \frac{\dot{w}_{in,i} + \dot{w}_{out,i}}{2} \quad (23)$$

Density ρ and flow rate \dot{w} were calculated values from the interpolation solution.

The transit-time correction was applied to equation (21) where $\dot{Q}_{fl,P}$ is evaluated at time $t_D + \sum_D^P t_{t,i}$, and $\dot{Q}_{fl,D}$ is evaluated at t_D . The left side of equation (21) may then be written as

$$\dot{Q}_{fl,P} - \dot{Q}_{fl,D} = \dot{Q}_{fl,P} \left(t_D + \sum_D^P t_{t,i} \right) - \dot{Q}_{fl,D}(t_D) \quad (24)$$

The transit time for the heat added in each increment $\dot{Q}_{m,i}$ to arrive at station P is different because of the location of the increment. Thus, the transit time correction for $\sum_D^P \dot{Q}_{m,i}$ is obtained by following a parcel of fluid through the system and determining the heat absorbed from the components at successively later times. Since the heat added near the inlet of an increment is added earlier to a fluid parcel than the heat added near the outlet of the increment, it is assumed that all the heat is added at one-half of the total transit time in the increment. In the following increments, however, the heat added in the preceding increment took the full transit time to go from in to out. The right side of equation (21) may then be written as follows:

$$\begin{aligned} \sum_D^P \dot{Q}_{m,i} = & \dot{Q}_{m,DE} \left(t_D + \frac{t_{t,DE}}{2} \right) + \dot{Q}_{m,EF} \left(t_D + t_{t,DE} + \frac{t_{t,EF}}{2} \right) \\ & + \dot{Q}_{m,FG} \left(t_D + t_{t,DE} + t_{t,EF} + \frac{t_{t,FG}}{2} \right) + \dots + \dot{Q}_{m,OP} \left(t_D + \sum_D^O t_t + \frac{t_{t,OP}}{2} \right) \end{aligned} \quad (25)$$

APPARATUS AND PROCEDURE

Facility and Research Systems

A description of the facility and research system is presented in reference 11. Figures 7 and 8 are photographs of the turbopump and reactor installations respectively, which are shown schematically in figure 1 (p. 7). Detailed descriptions of the turbopump, nozzle, and core are presented in references 1, 2, and 11, respectively.

The propellant used for the experiment was liquid hydrogen with a composition of approximately 97 percent para-hydrogen and 3 percent ortho-hydrogen as delivered. (Hydrogen property values used in the analysis were based on 99.79 percent para-hydrogen tabulated values from ref. 12 and were considered adequate since the results are calculated from enthalpy differences rather than from absolute values.)

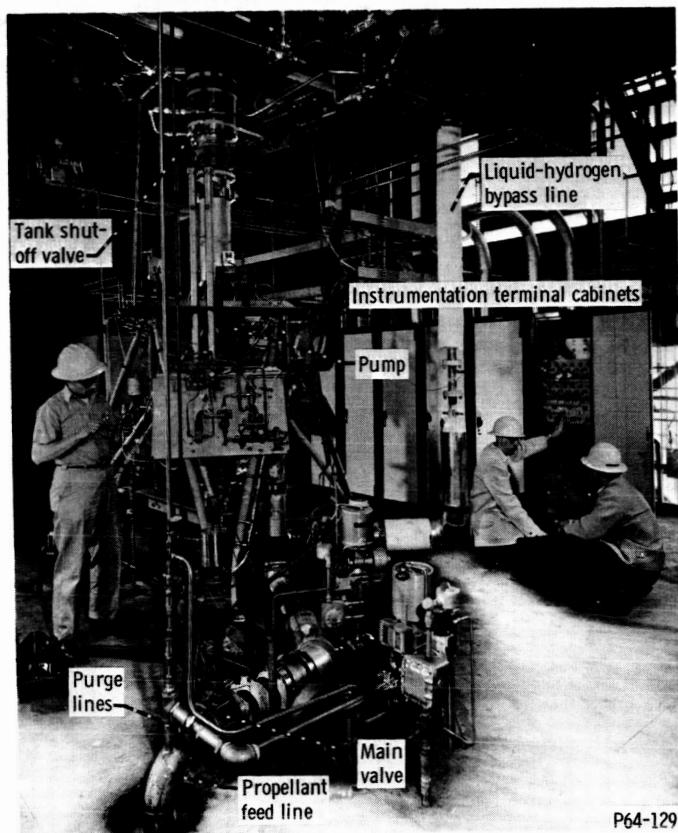


Figure 7. - Liquid-hydrogen turbopump installation.

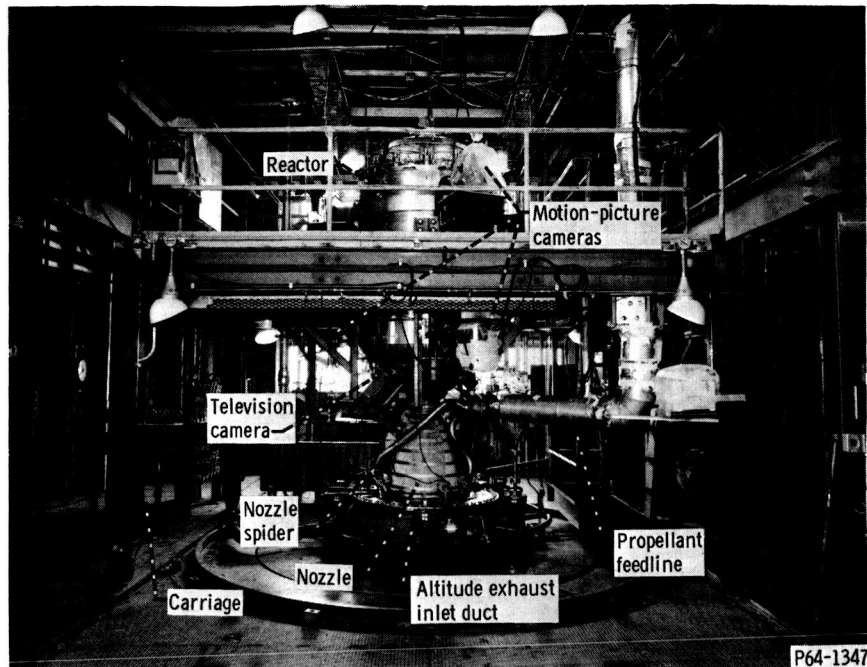


Figure 8. - Hydrogen feedline, nozzle, and reactor.

Instrumentation

The location of the experimental measurements is shown in figures 1 and 9 to 13. Only those measurements used for the data are presented. An identification item number consisting of prefix letters and a number was assigned to each measurement to simplify locating where the measurement was made. The prefix letters indicate location and type of measurement as shown in table II. A brief description of the various measurements used is discussed in the following paragraphs. Additional discussion on problem areas and accuracy is presented in appendix B.

Data from a turbine-type flowmeter located below the tank discharge opening (fig. 9) were used for the flow rate entering the system. Strain-gage-type differential pressure transducers were used for pressure measurements. Fluid temperatures were measured with platinum resistance thermometers when accessibility permitted it. They were calibrated for either a wide or narrow range of temperatures. Copper-constantan thermocouples were used for some fluid-temperature measurements and for all the component material temperatures.

Another important measurement was fluid density, which was obtained at station I by using a three-dimensional matrix capacitor. The capacitance of the sensor varies with the average dielectric constant of the fluid passing through it. Use of the Clausius-Massotti function (ref. 13), which relates density to dielectric constant, then enables

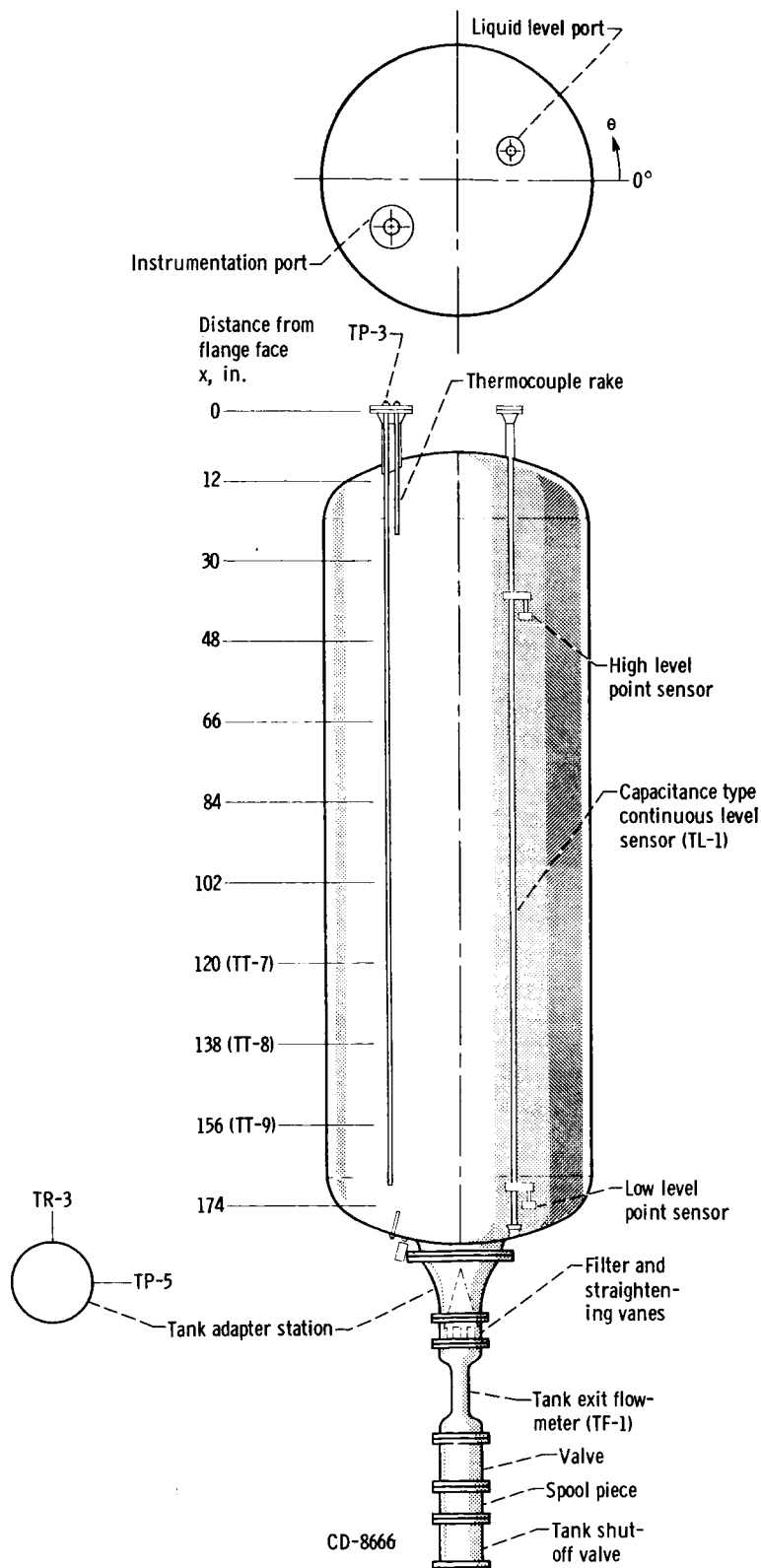


Figure 9. - Tank instrumentation.

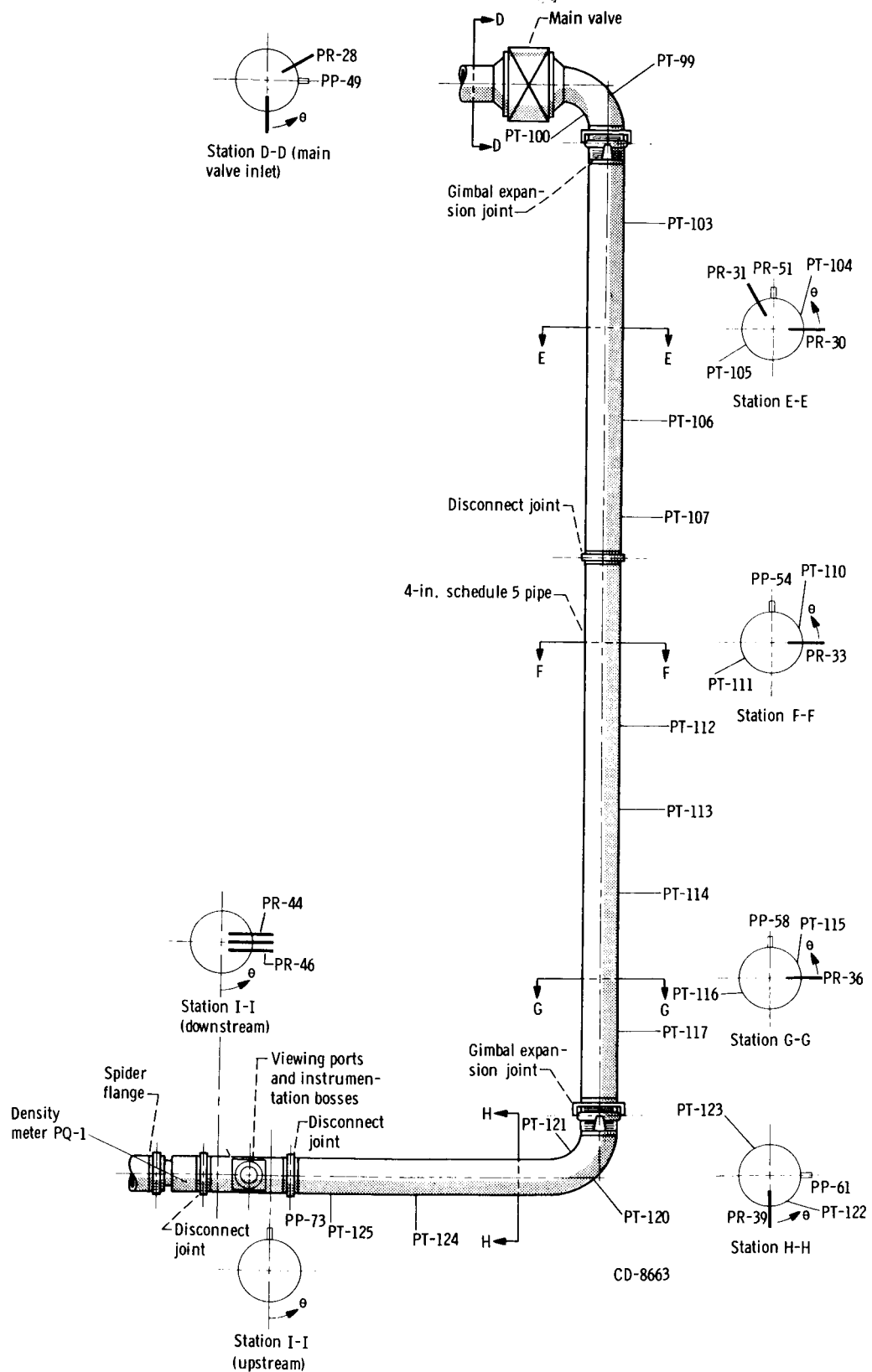


Figure 10. - Feedline instrumentation.

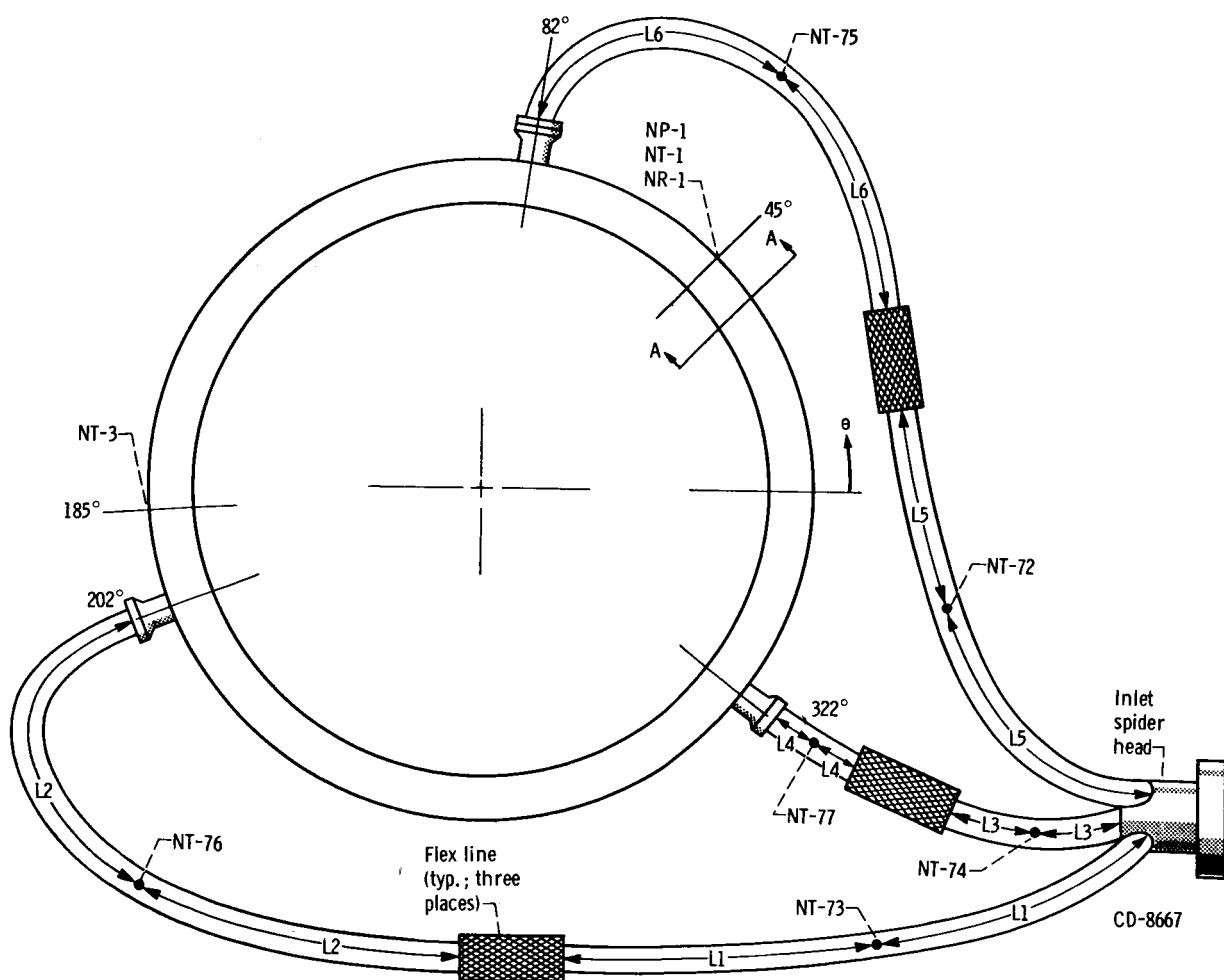
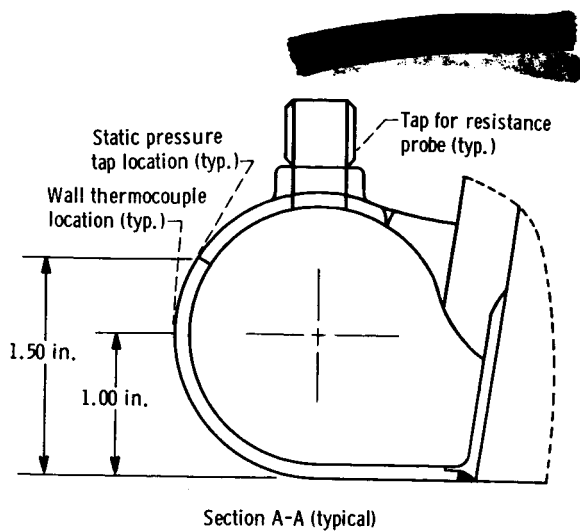


Figure 11. - Spider and nozzle tube inlet manifold (station J) instrumentation. (L1 \cong 11.0 in.; L2 \cong 8.0 in.; L3 \cong 5.5 in.; L4 \cong 6.5 in.; L5 \cong 11.0 in.; L6 \cong 8.0 in.)

CONFIDENTIAL

Component	Item	Distance from nozzle top, x, in.	Angular measurement, θ , deg
Tube 93	NP-7	3.50	185 ↓
	NP-8	12.50	
	NP-9	25.70	
	NP-10	45.25	
	NP-11	55.00	
Chamber	NP-50	12.24	140 320
	NP-51	12.24	
Tube 93	NT-7	3.50	185 ↓
	NT-9	19.10	
	NT-10	25.70	
	NT-13	36.00	
	NT-14	45.25	
Tube 23	NT-17	3.50	45 ↓
	NT-19	19.10	
	NT-20	25.70	
	NT-23	36.00	
Tube 178	NT-26	12.50	355 355 355
	NT-31	36.00	
	NT-32	45.25	
Nozzle shell	NT-39	12.50	185
	NT-40	19.10	185
Throat ring	NT-56	25.70	355
Instrumentation rake	NT-60	3.50	22
	NT-61	↓	22
	NT-62	↓	22
	NT-63	↓	202
	NT-64	↓	202

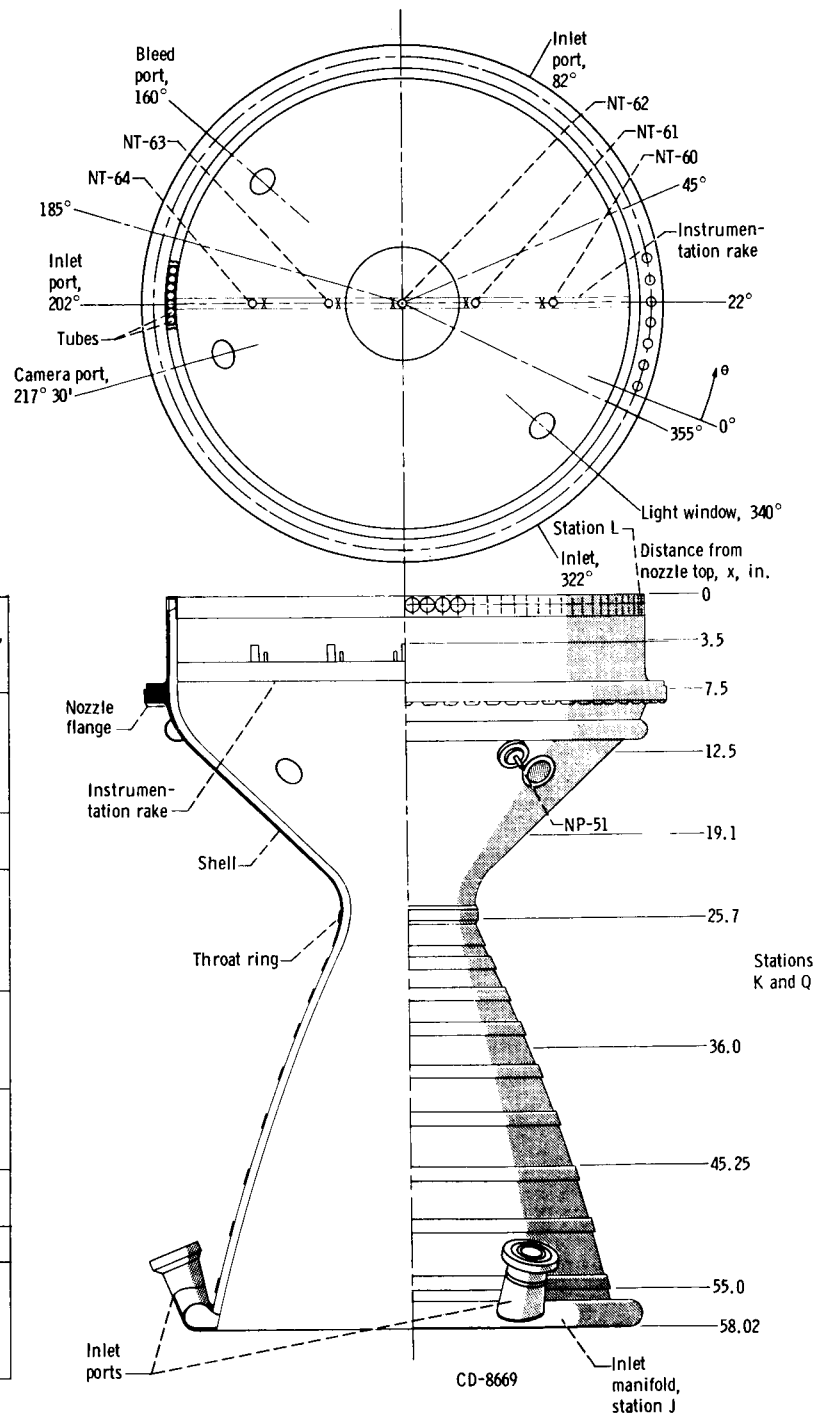


Figure 12. - Nozzle instrumentation.

CONFIDENTIAL

Component	Group	Type of measurement	Item	Distance from top of core z, in.	Angular measurement, θ , deg	Radius, in.
Reflector inlet plenum	---	Static pressure	RP-141	53	150	----
		Fluid temperature	RT-610 RR-612	53	235	----
Control rod edge	1	Material temperature	RT-266	2.25	See section B-B	----
			RT-267	28.25	See section B-B	----
			RT-268	50.25	See section B-B	----
Control rod center	2	Material temperature	RT-263	2.25	0	----
			RT-264	28.25	0	----
			RT-265	50.25	0	----
Control rod edge	3	Material temperature	RT-269	2.25	See section B-B	----
			RT-270	28.25	See section B-B	----
			RT-271	50.25	See section B-B	----
Pressure shell	4	Material temperature	RT-388	1.50	350	----
			RT-389	28.50	350	----
			RT-390	51.50	350	----
Graphite cylinder	5	Material temperature	RT-97	49.38	350	----
Main reflector segments	6	Static pressure	RP-66	13.25	168.3	23.41
			RP-68	36.25	168.3	23.41
	7	Material temperature	RT-104	1.25	350.7	23.87
			RT-106	28.25	350.7	23.87
			RT-109	51.25	350.7	23.87
	8	Material temperature	RT-116	1.25	346	23
			RT-118	28.25	346	23
			RT-121	51.25	346	23
	9	Material temperature	RT-110	1.25	348.8	21.34
			RT-136	28.25	48.8	21.34
Reflector outlet plenum	---	Static pressure	RP-146	-3.0	160	----
			---	---	---	---
	---	Fluid temperature	RR-619	-3.0	45	----
			RT-622 RR-624	-3.0	115 235	----
Flow separator	---	Static pressure	RP-121	-10.0	180	16
			---	---	---	---
	---	Fluid temperature	RT-349	-6.75	342	17
			RT-350	-6.75	162	17
			RT-353	-8.25	354	5.5
			RT-354	-8.25	174	5.5
Support plate	---	Fluid temperature	RT-342	-3.12	0	0
			RT-343	↓	16	5.3
			RT-344	↓	22	9.7
			RT-345	↓	18	11.3
			RT-392	↓	19	17.1
	---	Material temperature	RT-336	-3.12	180	0.85
			RT-339	-3.12	29	17.1
Fuel element, inlet plenum	---	Static pressure	RP-32	0.25	15	8.2
Fuel elements	11	Static pressure	RP-2	10.41	75	9.5
			RP-3	18.23	75	9.5
			RP-4	33.86	75	9.5
			RP-5	49.5	75	9.5
Modules	12	Material temperature	RT-31	3.11	180	0.62
			RT-32	10.92	↓	↓
			RT-33	18.73	↓	↓
			RT-34	34.36	↓	↓
			RT-35	50.0	↓	↓
Fuel elements	13	Material temperature	RT-1	1.0	75	0.17
			RT-2	8.81	↓	↓
			RT-3	16.63	↓	↓
			RT-4	32.26	↓	↓
			RT-5	47.90	↓	↓

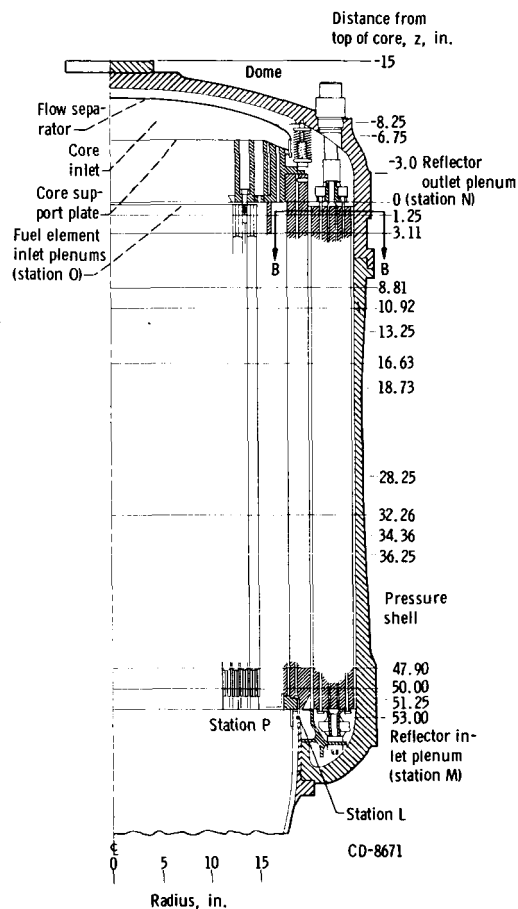
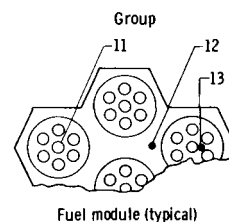
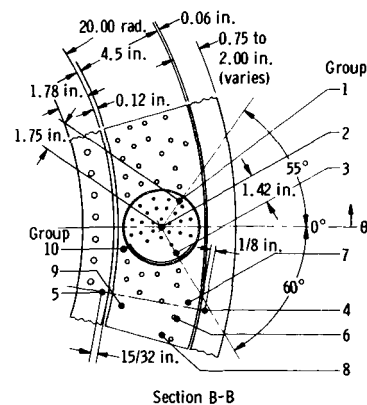


Figure 13. - Reactor instrumentation.

[REDACTED]

TABLE II. - INSTRUMENTATION CODE

First letter	Location	Second letter	Type of measurement
T	Tank	F	Flowmeter
P	Pump and piping	L	Liquid level
N	Nozzle	P	Pressure
R	Reactor	R	Resistance thermometer
		T	Thermocouple
		Q	Density

determination of the density of the fluid.

Data were recorded by digital and/or analog recording equipment. The digital recording equipment produced 100 channels of data at 10 outputs per second (each output was an average of 10 measurements) and 192 channels of data at about 3 outputs per second (each output was an average of seven measurements).

Test Procedure

A complete description of the test procedure is given in reference 11. The following discussion presents some of the highlights.

Before the run tank was filled with liquid hydrogen, the tank, the pump, and the feed-lines upstream of the main valve (see fig. 1, p. 7) were evacuated and purged three times with helium. The tank was then filled with 1800 gallons of liquid hydrogen.

Since the turbopump used had to be chilled to liquid-hydrogen temperature before rotating, the tank shutoff valve was opened and liquid hydrogen was allowed into the system up to the main valve. After about an hour (required to cool the heavy weight piping, etc.) of cold soak, the pump was at operating temperature and the test could begin.

The steam ejector system was started, and when the nozzle pressure was down to 3 pounds per square inch absolute, the automatic sequencer was initiated. A 30-second helium purge of the engine and nitrogen purge of the ejector were made and the run tank pressurization system ramped the tank pressure to the predetermined level. At this point, the steam ejector system has reduced the nozzle pressure to 0.5 pound per square inch absolute or less, and the data-acquisition systems had been sequenced on. Flow of hydrogen through the system was initiated from the controlled opening (full open in about 1 sec) of the main valve. Time zero ($t = 0$) on all the runs corresponds to the time when the main valve began opening.

For most of the runs, a finite length of time was allowed after flow was initiated at the main valve before opening the turbine-power control valve to start bootstrapping. The waiting period was allowed for stabilization of flow and pressure oscillations result-

ing from the initial surge of liquid into the system downstream from the main valve. The test was terminated by a manual initiation of the shutdown sequencer when it was determined that the test objectives had been met. After the pump stopped rotating, the tank shutoff valve was closed and the system was completely purged.

RESULTS AND DISCUSSION

Four runs (11, 19, 20, and 24) were selected for analysis from 26 chilldown runs made with the full-scale simulated system. These particular runs were selected because they covered a range of flow and flow acceleration rates that might be used during startup of a nuclear rocket. Another selection criterion was that flow and pressure oscillations be at a minimum so that the heat-transfer analysis would not be compromised by system dynamic effects, since the calculation procedure was not intended to handle the dynamics of two-phase flow. The true physical situation would be more closely simulated by a model such as that used in reference 8. All the runs had some oscillations, however, in the first few seconds of the run immediately following the opening of the main valve. No pump stall occurred in the chosen runs except for a very brief period during run 24.

The operating conditions and some system performance characteristics are summarized briefly in table III. The tank pressure setting establishes the rate of increase and magnitude of flow rate in the system prior to bootstrapping with the turbopump. The turbine-power control-valve delay time is the time elapsed before bootstrapping begins after initiation of flow at the main valve. The degree of chilldown of system components before bootstrapping varies with this delay time. The pump speed control setting (rpm/sec) establishes the rate of change of flow rate and pressure during the bootstrap

TABLE III. - OPERATING CONDITIONS AND SYSTEM
PERFORMANCE CHARACTERISTICS

Run	Nominal tank pressure, psia	Turbine-power control-valve opening delay time, sec	Pump speed control, rpm/sec	Maximum pump discharge pressure, psia	Time to maximum pressure, sec	Chilldown hydrogen used (up to maximum pressure time), lb
11	50	10.5	500	91	23	228
19	35	6.5	200	60	28	224
20	25	10.5	100 and 300 at 42 sec	51	48	282
24	35	0.1	Turbine-power control valve wide open	142	12	180

TABLE IV. - EXPERIMENTAL DATA FOR RUN 24

Time, t, sec	Station												
	D		E		F		G		H		I		
	Item												
	TF-1	PP-34	PR-28	Material heat flow rate, $\frac{E}{D} \sum \dot{Q}_m'$ Btu/sec	PP-51	Material heat flow rate, $\frac{F}{E} \sum \dot{Q}_m'$ Btu/sec	PP-54	Material heat flow rate, $\frac{G}{F} \sum \dot{Q}_m'$ Btu/sec	PP-58	Material heat flow rate, $\frac{H}{G} \sum \dot{Q}_m'$ Btu/sec	PP-61	Material heat flow rate, $\frac{I}{H} \sum \dot{Q}_m'$ Btu/sec	PP-73
Flow rate, \dot{w}_D' lb/sec	Static pressure, $P_{s,D}'$ psia	Fluid temper- ature, $T_{f,D}'$ °R	Material heat flow rate, $\frac{E}{D} \sum \dot{Q}_m'$ Btu/sec	Static pressure, $P_{s,E}'$ psia	Material heat flow rate, $\frac{F}{E} \sum \dot{Q}_m'$ Btu/sec	Static pressure, $P_{s,F}'$ psia	Material heat flow rate, $\frac{G}{F} \sum \dot{Q}_m'$ Btu/sec	Static pressure, $P_{s,G}'$ psia	Material heat flow rate, $\frac{H}{G} \sum \dot{Q}_m'$ Btu/sec	Static pressure, $P_{s,H}'$ psia	Material heat flow rate, $\frac{I}{H} \sum \dot{Q}_m'$ Btu/sec	Static pressure, $P_{s,I}'$ psia	Density, ρ , lb/cu ft
0	35.2	42.93	-----	0.5	0.5	0.5	0.5	0.5	-----	0.5	-----	-----	0.0303
.336	2.17	34.87	29.96	32.14	25.64	32.15	26.34	32.34	18.50	32.30	19.26	32.42	.0291
.672	2.31	33.04	55.70	31.45	70.24	31.26	72.56	31.48	57.48	31.64	62.71	31.52	.0431
1.008	3.12	38.97	51.80	39.58	73.13	39.39	78.07	39.83	62.76	39.69	74.33	39.50	.1591
1.344	5.40	29.37	31.52	28.10	57.60	27.81	69.96	28.21	62.27	28.42	74.67	27.95	.1105
1.680	3.70	31.32	33.66	30.72	50.78	30.31	59.08	30.62	53.36	30.72	66.33	30.54	.0734
2.016	4.59	28.71	29.51	27.47	40.10	27.24	47.82	27.49	47.51	27.79	59.91	27.52	.1685
2.352	5.16	30.31	25.98	29.83	35.36	29.54	41.79	29.93	43.77	29.88	56.92	29.59	.1917
2.688	5.74	30.43	24.62	30.04	34.38	29.80	39.98	30.19	38.08	30.09	47.24	29.65	.3118
3.024	6.25	30.82	25.34	30.44	31.94	30.08	37.12	30.28	37.43	30.26	47.41	30.00	.3762
3.360	6.54	31.98	22.47	31.88	29.52	31.55	36.62	31.94	35.34	32.13	43.96	31.84	.4785
3.696	6.90	33.78	21.74	33.49	26.06	32.96	30.69	33.49	31.68	33.62	40.18	33.37	.855
4.032	6.72	37.42	22.65	37.33	28.07	37.06	29.32	37.59	29.52	37.56	37.66	37.43	1.091
4.368	6.80	40.35	23.52	40.10	27.54	39.71	30.41	40.08	27.72	40.20	33.63	39.79	1.070
4.704	7.97	42.01	22.19	41.51	24.90	41.46	29.46	41.95	26.73	41.93	30.75	41.69	1.635
5.040	8.35	45.94	23.33	45.46	28.26	45.22	30.57	45.85	25.73	45.81	32.18	45.72	2.170
5.376	8.85	50.35	24.47	49.84	29.80	49.53	31.57	50.10	25.51	49.97	31.64	49.89	2.565
5.712	8.73	55.43	23.10	54.83	33.07	54.44	35.80	55.03	27.31	55.12	31.96	55.22	2.820
6.048	9.27	58.32	23.71	57.46	34.05	57.00	35.08	57.61	26.56	57.90	34.42	57.41	3.245
6.384	9.69	63.00	22.38	62.36	34.98	61.80	40.72	62.81	28.07	62.70	34.32	62.56	3.373
6.720	10.71	66.87	22.74	65.82	39.25	65.44	41.08	66.16	29.19	66.15	38.02	65.87	3.520
7.056	11.96	71.71	20.69	70.35	39.32	69.84	50.24	70.67	28.11	70.38	35.98	70.22	3.770
7.392	14.08	89.14	20.05	87.21	43.80	86.38	46.70	87.99	31.49	87.36	40.94	87.12	3.912
7.728	19.14	114.20	11.32	109.07	50.93	108.33	57.22	109.85	34.40	109.00	48.17	108.89	4.000
8.064	23.04	130.45	.38	124.33	44.66	123.18	71.84	124.79	34.79	123.79	37.19	123.37	4.080
8.400	26.14	137.79	.02	130.44	1.28	129.30	7.37	130.85	6.62	129.74	1.39	129.51	4.210
8.736	28.17	142.81	.03	133.47	.28	132.08	1.04	133.57	.51	133.05	.31	132.21	4.240
9.072	29.74	140.58	-----	129.67	0	128.50	.23	129.93	.09	129.52	.10	128.82	4.240
9.408	30.07	138.65	-----	127.62	.02	126.54	-----	127.81	.10	127.30	.12	126.60	4.225

TABLE V. - CALCULATED FLUID CONDITIONS FOR RUN 24

Time, t, sec	Station																		
	D	E					F					G					H		
		Enthalpy, h_D , Btu/lb	Enthalpy, h_E , Btu/lb	Fluid temper- ature, $T_{fl,E}$, $^{\circ}R$	Flow rate, \dot{w}_E , lb/sec	Density, ρ_E , lb/cu ft	Enthalpy, h_F , Btu/lb	Fluid temper- ature, $T_{fl,F}$, $^{\circ}R$	Flow rate, \dot{w}_F , lb/sec	Density, ρ_F , lb/cu ft	Enthalpy, h_G , Btu/lb	Fluid temper- ature, $T_{fl,G}$, $^{\circ}R$	Flow rate, \dot{w}_G , lb/sec	Density, ρ_G , lb/cu ft	Enthalpy, h_H , Btu/lb	Fluid temper- ature, $T_{fl,H}$, $^{\circ}R$	Flow rate, \dot{w}_H , lb/sec	Density, ρ_H , lb/cu ft	
<0	-92	1422	434	0	0.0002	1650	497	0	0.0002	1655	498	0	0.0002	1670	502	0	0.0002		
.336	-94	897	297	.98	.02	942	308	.98	.0162	968	314	.98	.0190	988	320	.98	.0187		
.672	-94	-63	42	1.31	.81	10	42	1.18	.273	87	41.5	1.16	.168	125	53	1.16	.120		
1.008	-91	-71	43	2.04	1.35	-22	41	1.87	.495	28	43.5	1.85	.365	76	43	1.76	.220		
1.344	-97	-89	41	2.62	1.82	-58	40	2.13	.590	-10	40.8	1.97	.298	24	40.8	1.73	.222		
1.680	-96	-86		2.70	1.70	-59	41	2.30	.685	-27	41.6	2.08	.409	3	41.1	1.95	.285		
2.016	-98	-90		3.03	1.80	-71	40	2.63	.810	-51	40.3	2.44	.518	-29	40.4	2.23	.365		
2.352	-97	-91		3.84	2.25	-80	41	3.42	1.170	-65	41.3	3.19	.795	-48	41.0	2.95	.530		
2.688	-97	-92		4.63	2.40	-83	41	4.14	1.47	-71	41.3	3.85	.920	-60	41.1	3.57	.700		
3.024	-97	-93		5.48	2.80	-86	41	4.96	1.69	-77	41.3	4.62	1.14	-67	41.1	4.31	.840		
3.360	-96	-93	42	6.16	3.15	-87	42	5.65	1.92	-79	41.8	5.28	1.36	-71	41.8	4.96	1.01		
3.696	-97	-94	42	6.90	3.80	-90	42	6.39	2.45	-85	42.0	5.98	1.87	-79	41.9	5.65	1.38		
4.032	-98	-95	42	6.72	4.15	-90	43	6.61	3.38	-85	43.1	6.27	2.38	-79	42.9	6.01	1.70		
4.368	-100	-97	41	6.80	4.20	-94	42	6.80	4.16	-85	43.5	6.63	3.45	-84	43.5	6.40	2.50		
4.704	-101	-98		7.97	4.22	-95		7.97	4.16	-91	43	7.97	4.12	-87	43.7	7.70	3.25		
5.040		-97		8.35	4.22	-94		8.35	4.17	-90	44	8.35	4.08	-87	44	8.35	4.08		
5.376		-97		8.85	4.22			8.85	4.18	-90		8.85	4.08	-87	44	8.85	4.07		
5.712		-97		8.73	4.22			8.73	4.18	-89		8.73	4.09	-86	45	8.73	4.06		
6.048		-97		9.27	4.23			9.27	4.19	-90		9.27	4.09	-87	44	9.27	4.07		
6.384		-98		9.69	4.24			9.69	4.20	-90		9.69	4.10	-87		9.67	4.08		
6.720		-98		10.71	4.25			10.71	4.21	-90	43	10.71	4.12	-88		10.71	4.09		
7.056				11.96	4.26	-95		11.96	4.22	-92	43	11.96	4.16	-89		11.96	4.10		
8.064	-100	-99	40	14.08	4.30	-94		14.08	4.22	-91	43	14.08	4.18	-89		14.08	4.13		
9.072	-99	-99	40	19.14	4.32	-96	41	19.14	4.28	-93	42	19.14	4.23	-91	43	19.14	4.18		
10.080	-98	-98		23.04	4.33	-96	41	23.04	4.31	-93	42	23.04	4.26	-91	43	23.04	4.22		
11.088				26.14		-98	40	26.14	4.33	-98	40	26.14	4.33	-97	40	26.14	4.32		
12.096				28.17		-98	40	28.17	4.33	-98	40	28.17	4.33	-98	40	28.17	4.33		
13.104				29.74		-98	40	29.74	4.33	-98	40	29.74	4.33	-98	40	29.74	4.33		
13.440				30.07		-98	40	30.07	4.33	-98	40	30.07	4.33	-98	40	30.07	4.33		

TABLE V. - Continued. CALCULATED FLUID CONDITIONS FOR RUN 24

Time, t, sec	Station															
	I				J				K				L			
	Enthalpy, h_I , Btu/lb	Fluid temper- ature, $T_{fI,I}$, $^{\circ}R$	Flow rate, \dot{w}_I , lb/sec	Density, ρ_I , lb/cu ft	Enthalpy, h_J , Btu/lb	Fluid temper- ature, $T_{fI,J}$, $^{\circ}R$	Flow rate, \dot{w}_J , lb/sec	Density, ρ_J , lb/cu ft	Enthalpy, h_K , Btu/lb	Fluid temper- ature, $T_{fI,K}$, $^{\circ}R$	Flow rate, \dot{w}_K , lb/sec	Density, ρ_K , lb/cu ft	Enthalpy, h_L , Btu/lb	Fluid temper- ature, $T_{fI,L}$, $^{\circ}R$	Flow rate, \dot{w}_L , lb/sec	Density, ρ_L , lb/cu ft
<0	1677	504	0	0.0002	1695	509	0	0.0002	1710	513	0	0.0002	1724	517	0	0.0002
.336	1007	324	.98	.0184	1019	327	.98	.0177	1513	464	.98	.0069	1717	515	.98	.0022
.672	179	75	1.16	.0820	358	143	1.16	.0395	1079	343	1.16	.0109	1421	433	1.16	.0048
1.008	108	50	1.71	.171	319	125	1.71	.0575	805	272	1.71	.0172	1084	345	1.71	.0081
1.344	136	55	1.27	.102	482	184	1.27	.0275	867	288	1.27	.0117	1091	347	1.27	.0070
1.680	77	42	1.57	.175	360	144	1.53	.0380	600	227	1.53	.0157	800	272	1.53	.0090
2.016	43	40.7	1.68	.195	380	151	1.34	.0325	527	197	1.34	.0161	680	240	1.34	.0101
2.352	-12	41.0	2.39	.330	250	103	1.74	.0535	392	155	1.74	.0218	550	202	1.74	.0150
2.688	-36	41.0	2.94	.453	218	90	1.89	.0608	323	130	1.89	.0275	445	171	1.89	.0195
3.024	-47	41.1	3.68	.542	168	70	2.24	.0792	236	97	2.24	.0365	371	147	2.24	.0244
3.360	-57	42.0	4.35	.710	131	57	2.62	.109	179	74	2.62	.054	289	118	2.62	.0355
3.696	-68	42.0	5.07	.952	78	41.7	3.19	.180	111	47	3.03	.105	192	79.5	3.03	.055
4.032	-72	42.9	5.57	1.28	41	42.8	4.14	.256	58	40.8	3.92	.207	134	57.5	3.77	.099
4.368	-78	43.5	6.05	1.80	7	43.3	4.85	.350	12	41.7	4.67	.280	68	41.9	4.52	.198
4.704	-82	44.0	7.23	2.42	-14	43.7	5.59	.470	-11	42.1	5.35	.370	44	42.3	5.10	.242
5.040	-83	44.6	7.94	2.73	-29	44.5	6.38	.640	-27	43.3	6.27	.527	17	43.2	6.00	.324
5.376	-83	45.3	8.71	3.50	-39	45.3	7.36	.824	-38	44.1	7.17	.68	1	44.0	6.89	.415
5.712	-83	45.8	8.73	3.95	-46	46.1	7.92	1.05	-46	45.1	7.80	.92	-8	45.0	7.60	.51
6.048	-84	45.5	9.27	4.00	-52	46.5	8.55	1.28	-52	45.4	8.42	1.08	-20	45.3	8.19	.64
6.384	-83	45.7	9.67	4.00	-57	47.3	9.27	1.64	-57	46.4	9.18	1.43	-27	46.1	8.98	.78
6.720	-84	45.5	10.71	4.02	-61	47.8	10.33	2.00	-61	46.8	10.20	1.71	-33	46.3	9.92	.91
7.056	-86	44.9	11.96	4.03	-68	48.3	11.68	2.75	-68	47.4	11.53	2.44	-44	47.2	11.17	1.22
8.064	-86	44.8	14.08	4.07	-72	48.8	14.08	3.78	-72	48.8	14.08	3.76	-53	49.8	13.97	2.10
9.072	-88	44.0	19.14	4.15	-78	47.1	19.14	3.95	-78	47.1	19.14	3.95	-62	51.1	19.14	3.62
10.080	-90	43.2	23.04	4.21	-87	44.2	23.04	4.16	-87	44.3	23.04	4.15	-74	48.2	23.04	3.88
11.088	-97	40.6	26.14	4.31	-97	40.6	26.14	4.30	-97	41.7	26.14	4.28	-86	44.6	26.14	4.14
12.096	-98	40.1	28.17	4.33	-98	40.2	28.17	4.32	-98	40.3	28.17	4.32	-87	44.2	28.17	4.15
13.104	-98	40.1	29.74	4.33	-98	40.2	29.74	4.32	-98	40.4	29.74	4.31	-88	44.0	29.74	4.15
13.440	-98	40.2	30.07	4.32	-98	40.2	30.07	4.32	-98	40.4	30.07	4.31	-89	43.6	30.07	4.18

TABLE V. - Concluded. CALCULATED FLUID CONDITIONS FOR RUN 24

Time, t , sec	Station															
	M				N				O				P			
	Enthalpy, h_M , Btu/lb	Fluid temper- ature, $T_{fl,M}$, $^{\circ}R$	Flow rate, \dot{w}_M , lb/sec	Density, ρ_M , lb/cu ft	Enthalpy, h_N , Btu/lb	Fluid temper- ature, $T_{fl,N}$, $^{\circ}R$	Flow rate, \dot{w}_N , lb/sec	Density, ρ_N , lb/cu ft	Enthalpy, h_O , Btu/lb	Fluid temper- ature, $T_{fl,O}$, $^{\circ}R$	Flow rate, \dot{w}_O , lb/sec	Density, ρ_O , lb/cu ft	Enthalpy, h_P , Btu/lb	Flow rate, \dot{w}_P , lb/sec	Density, ρ_P , lb/cu ft	Flow rate, \dot{w}_Q , lb/sec
<0	1729	518	0	0.0002	1728	518	0	0.0002	1738	521	0	0.0002	1732	0	0.0002	0
.336	----	---	.98	-----	1720	516	.98	.0021	1742	522	.98	.0004	1735	.98	.0010	.98
.672	1590	480	1.16	.0039	1722	516	1.16	.0023	1739	521	1.16	.0013	1738	1.16	.0012	1.16
1.008	1217	379	1.71	.0075	1727	518	1.71	.0034	1736	520	1.71	.0020	1742	1.71	.0017	1.71
1.344	1299	401	1.27	.0047	1710	513	1.27	.0024	1718	515	1.27	.0022	1742	1.27	.0012	1.26
1.680	911	300	1.53	.0085	1709	513	1.53	.0030	1709	513	1.53	.0021	1742	1.53	.0015	1.52
2.016	842	282	1.34	.0078	1687	507	1.34	.0027	1694	509	1.34	.0021	1746	1.34	.0013	1.33
2.352	686	241	1.74	.0118	1691	508	1.74	.0035	1700	510	1.74	.0024	-----	1.74	.0017	1.73
2.688	587	215	1.89	.0132	1687	507	1.89	.0037	1698	510	1.89	.0027	-----	1.89	.0018	1.87
3.024	503	190	2.24	.0170	1687	507	2.24	.0042	1701	510	2.24	.0031	-----	2.24	.0022	2.22
3.360	420	164	2.62	.0241	1689	507	2.62	.0049	1704	511	2.62	.0035	-----	2.62	.0026	2.59
3.696	322	130	3.03	.0331	1677	504	3.03	.0056	1700	510	3.03	.0041	-----	3.03	.0030	2.99
4.032	241	98.9	3.77	.0524	1671	502	3.77	.0069	1698	510	3.77	.0050	-----	3.77	.0036	3.71
4.368	178	74.8	4.34	.083	1654	498	4.34	.0079	1688	507	4.34	.0059	-----	4.34	.0042	4.27
4.704	165	69.9	4.61	.095	1626	490	4.61	.0085	1670	502	4.61	.0063	-----	4.61	.0044	4.52
5.040	117	52.7	5.35	.152	1599	482	5.35	.0099	1651	497	5.35	.0073	-----	5.35	.0051	5.25
5.376	88	44.0	6.09	.223	1564	473	6.09	.0114	1628	490	6.09	.0084	-----	6.09	.0058	5.96
5.712	57	45.1	7.09	.274	1531	463	6.96	.0131	1604	484	6.96	.0097	-----	6.96	.0067	6.82
6.048	40	45.3	7.64	.351	1461	444	7.35	.0146	1551	469	7.35	.0107	1742	7.35	.0071	7.19
6.384	24	46.3	8.58	.442	1441	439	8.25	.0162	1542	467	8.25	.0120	1739	8.25	.0079	8.08
6.720	16	46.7	9.40	.492	1384	423	8.84	.0178	1503	456	8.84	.0130	1735	8.84	.0085	8.64
7.056	-1	47.3	10.54	.566	1300	401	9.68	.0202	1435	437	9.68	.0148	1735	9.68	.0093	9.46
8.064	-27	49.6	13.71	1.18	1160	364	13.13	.0287	1309	403	13.13	.0213	1717	13.13	.0122	12.84
9.072	-39	52.1	18.98	2.07	1010	325	18.20	.043	1143	359	18.20	.0315	1674	18.20	.0178	17.77
10.080	-58	52.1	23.04	3.55	884	293	22.05	.0545	1009	326	22.05	.0404	1576	22.05	.0222	21.53
11.088	-73	48.4	26.14	3.87	780	267	24.68	.0615	901	297	24.68	.047	1430	24.68	.0265	24.10
12.096	-73	48.5	28.17	3.87	650	233	27.61	.0755	761	262	27.61	.056	1236	27.61	.0307	26.97
13.104	-71	49.0	29.74	3.83	560	208	29.49	.0845	665	236	29.49	.061	1017	29.49	.0359	28.85
13.440	-71	49.0	30.07	3.83	555	206	29.87	.083	657	234	29.87	.061	947	29.87	.0375	29.23

operation. The rate of rise of flow and pressure, however, are also affected by how much chilldown (or heat transfer) has occurred after opening the main valve and prior to start of bootstrap.

Run 24 was selected as being representative of a nuclear rocket startup transient when the pump is prechilled. Less hydrogen was used during the chilldown in this run because of the short time required for startup. Minimum quantities of hydrogen are desirable during chilldown because little propulsive energy is available from the hydrogen at the low fluid temperatures during this period. Close simulation of a nuclear heated engine startup is lost by the time maximum pump discharge pressure is reached in the chilldown tests. In a flight reactor startup, it would be required that the nuclear power ramp be sufficiently under way furnishing hot hydrogen at the core outlet by this time to enable continuous smooth bootstrap to full power operation.

Typical input data and detailed calculated results are presented for run 24 at the eleven stations between the inlet station D and the core outlet station P. The input data are presented in table IV and the calculated flow rates and fluid properties in table V. The effect of operating conditions on flow and fluid properties was determined for two stations (J and L) in runs 11, 19, and 20.

Experimental Input Data

Flow rate. - A plot of the flow rate entering the system and the flow rate leaving the system is presented in figure 14. Brief flow oscillations occurred in the first 2 seconds

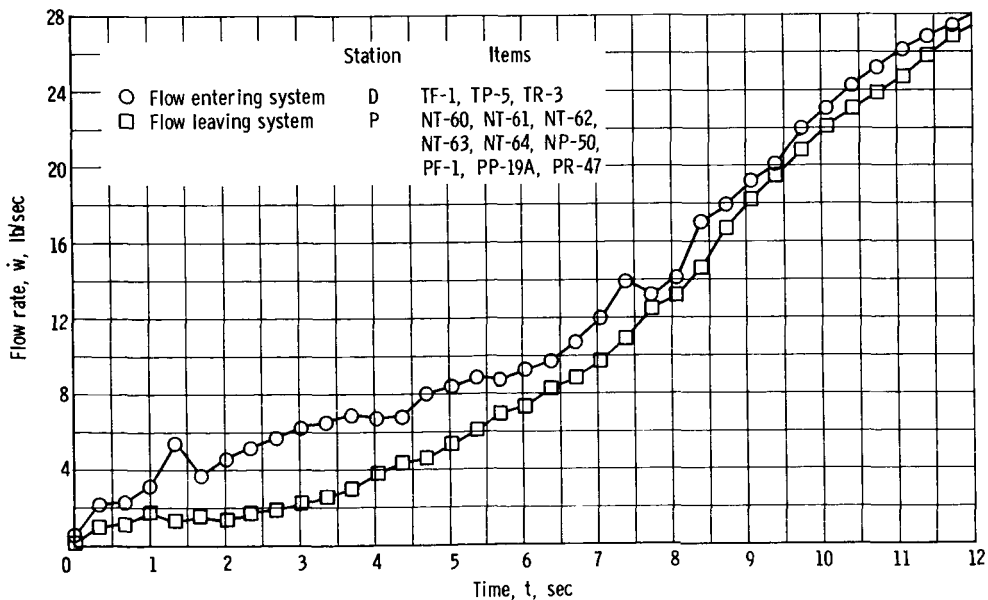


Figure 14. - Experimental flow rates for low-frequency data. Run 24.

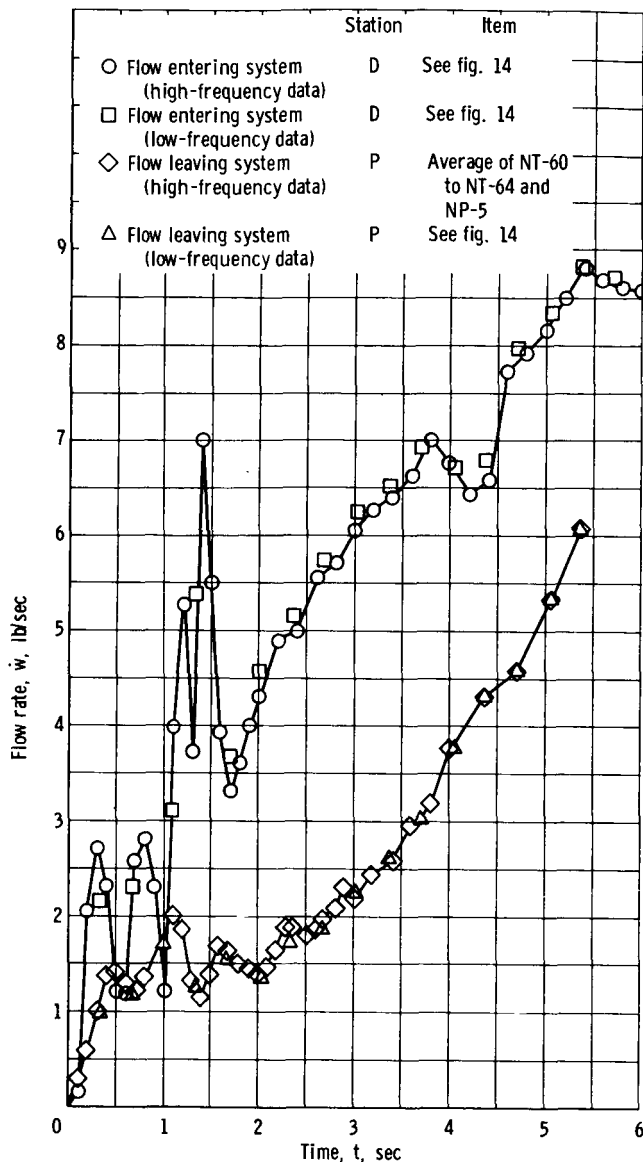


Figure 15. - Comparison of low- and high-frequency flow-rate data. Run 24.

and at 7.4 seconds. The first occurrence is typical of all runs and is the primary result of the initial surge of flow into the system when the main valve is opened. The second occurrence is at the time when the pump operated momentarily in the stall region.

The data shown in figure 14 were processed from the low-frequency digital data (approximately 3 outputs/sec) and considerable smoothing exists. The same data are shown in figure 15 with an enlarged scale where it is compared with data processed from the high-frequency digital system, which has a greater sampling rate (10 outputs/sec). The nature of the initial oscillations is seen more clearly in the high-frequency data, and the effect of the lower sampling rate is apparent. It appears that momentarily at 0.5 and 1.0 second the actual flow leaving the system was greater than the flow entering the system.

The transit time of perturbations through the system is evident by the approximate 0.25 second phase shift in the oscillations of the flow entering and leaving the system. After the first 2 seconds, the low-frequency data agree well with the high-frequency values.

For the heat-transfer-analysis method used, the low-frequency data were considered adequate, and high-frequency data were used only when low-frequency data were not available or were inaccurate.

Fluid pressure and temperature. - Experimental fluid pressure and temperature data are presented in figures 16 to 19 for run 24. The highly dynamic nature of the initial flow in the system is evident in the pressure and temperature data (figs. 16 and 17) in the first 2 seconds, after which the system is relatively stable.

The temperature data shown in figure 17 were not corrected for the time constant

~~CONFIDENTIAL~~

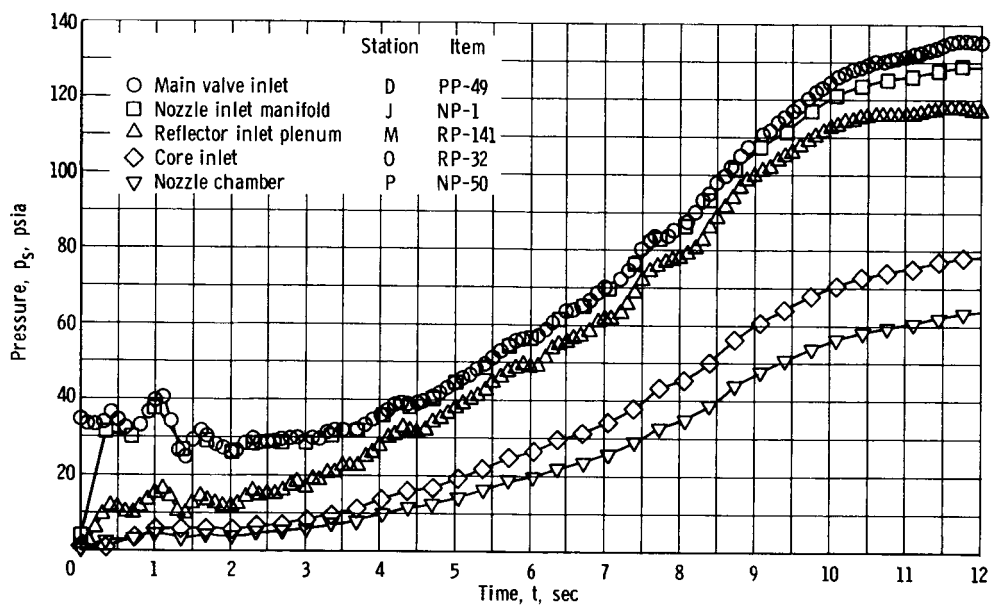


Figure 16. - Typical experimental pressure data. Run 24.

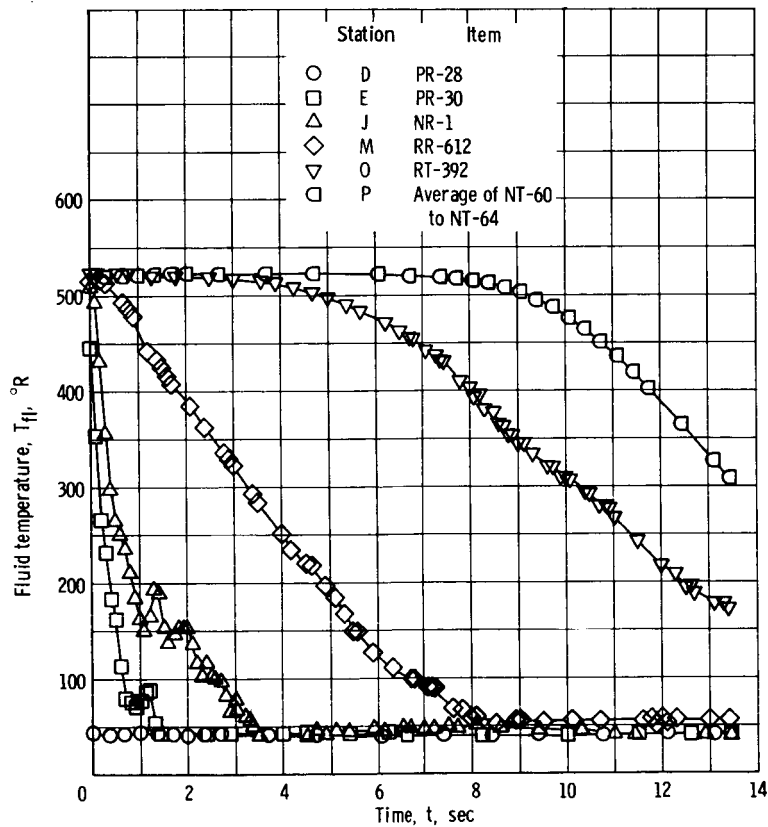


Figure 17. - Typical experimental indicated fluid temperature data. Run 24.

~~CONFIDENTIAL~~

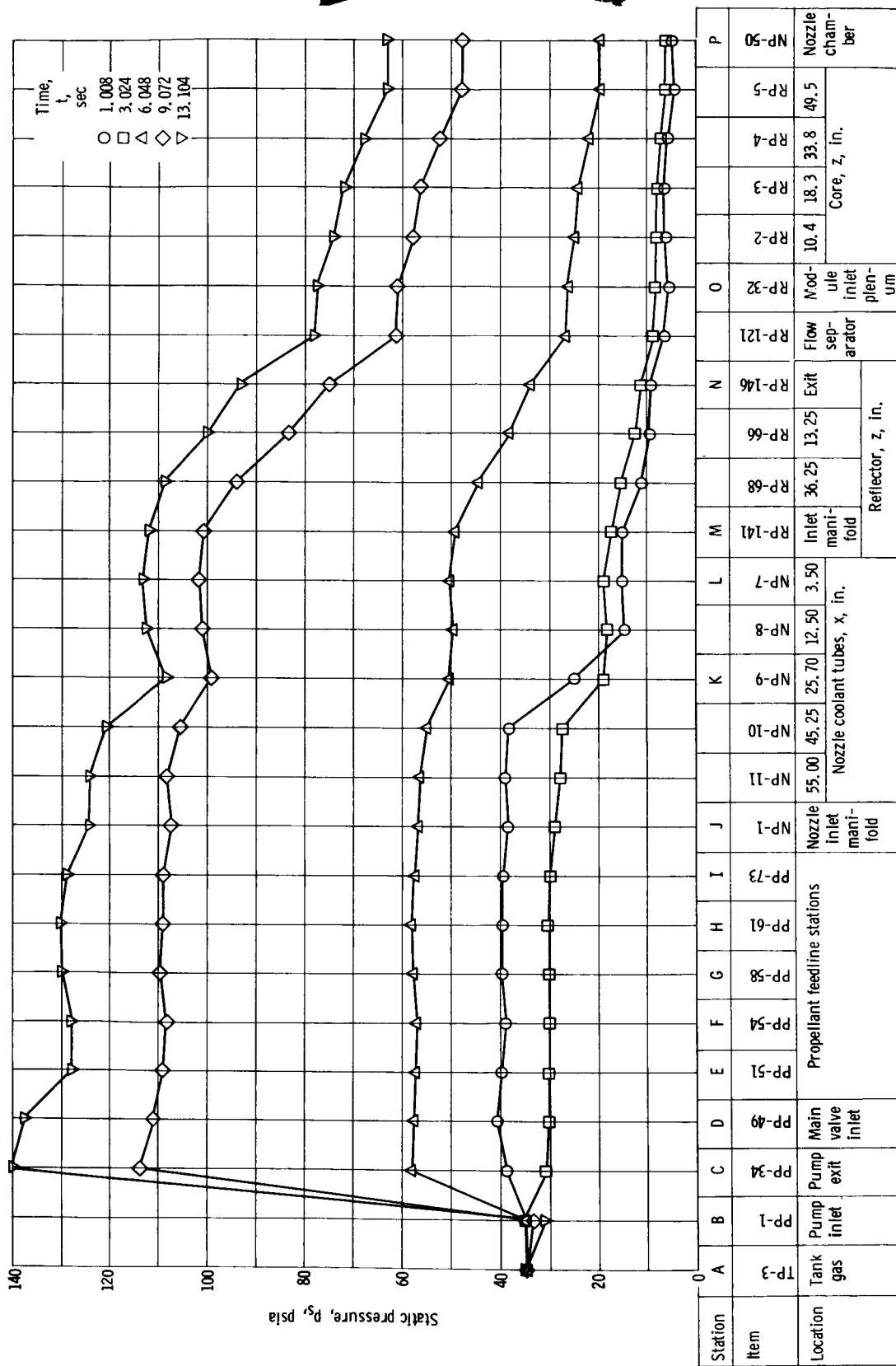


Figure 18. - Experimental pressure profile in system. Run 24.

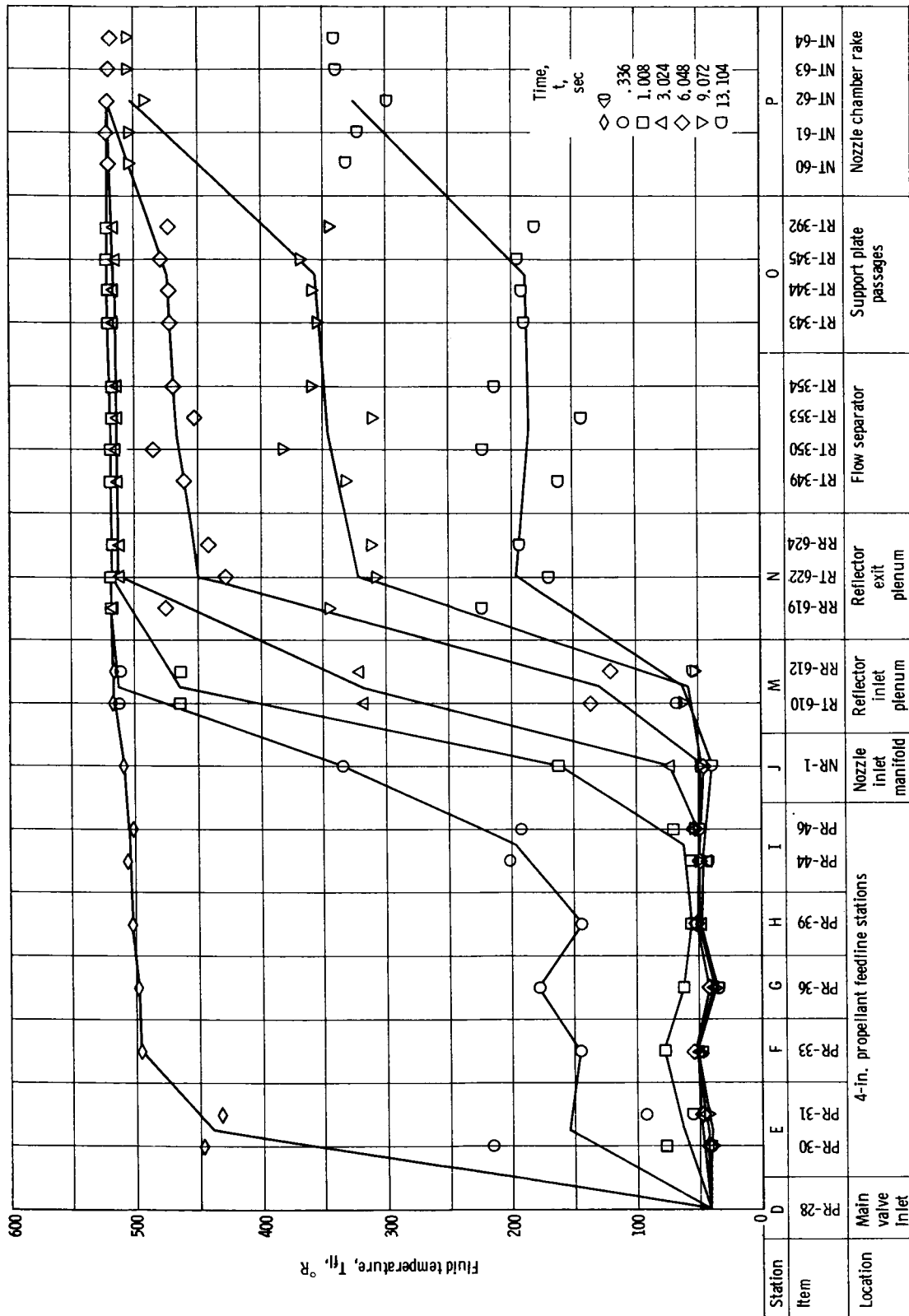


Figure 19. - Experimental indicated temperature profile in system, Run 24.

(not accurately known) of the sensors. The true temperatures at station E in the feedline and at the nozzle manifold (station J) were considerably lower than that indicated during the rapid transient (see appendix B).

Careful editing of the experimental pressure data was accomplished by using plots such as those shown in figure 18 for run 24. Calibration discrepancies were detected by comparing individual measurements with others at the same location and other stations nearby. Accurate pressures were desired because of the sensitivity of density to pressure in the low quality two-phase region.

The data shown in figure 18 also indicate that the maximum pressure drop occurs in different components at different times during the run. For example, the curve at 1 second shows a pressure drop exceeding the critical pressure ratio in the nozzle coolant tubes in the throat region. Later in the run, the maximum pressure drop occurs in the reflector. A slight pressure rise is noted in the propellant feedline at 13 seconds, which shows the influence of gravity head in the vertical section after it is full of liquid.

Large fluid temperature gradients in the system are shown in the data (uncorrected for time constant) plotted in figure 19. Early in the run, a gradient of several hundred degrees exists in the feedline; later the steep gradient exists in the nozzle and in the reflector. The scatter in the data is indicative of dynamic response errors early in the run (station E, e. g.) and temperature maldistributions later in the run (downstream of the reflector). The fluid temperature data were not used in the analysis except where \dot{Q}_m data were not available. Average temperature values were used when enthalpy differences were required to replace the missing \dot{Q}_m values (\dot{Q}_{NO} , run 24, e. g.).

Heat-transfer rates. - The rate of heat transfer from the material of the various component parts to the hydrogen was obtained from the average temperature of the components and the rate of change with time (eq. (14)). Typical average material temperature data used for this calculation are shown in figure 20. The slope of the various curves is a function of several factors such as specific heat of the material, weight of the component, heat-transfer area, heat-transfer coefficient, etc. The nozzle tubes, although located downstream of the feedline, cool faster because of the thinner wall and larger heat-transfer area. Likewise, the core cools faster than the main reflector because of the different material.

The temperature of the upper nozzle tubes increased with time for a short period after 7 seconds (fig. 20) and remained above 100°R for the balance of the run. Heat transfer from the warmer gas on the exhaust side of the coolant tubes accounts for the high temperature.

A summary of the heat-transfer rate from each of the major components and from the total system is presented in figure 21. Components near the upstream end, where liquid hydrogen enters the system, such as the feedline and the nozzle, transfer heat rapidly near the beginning of the run and relatively slowly near the end of the run when most

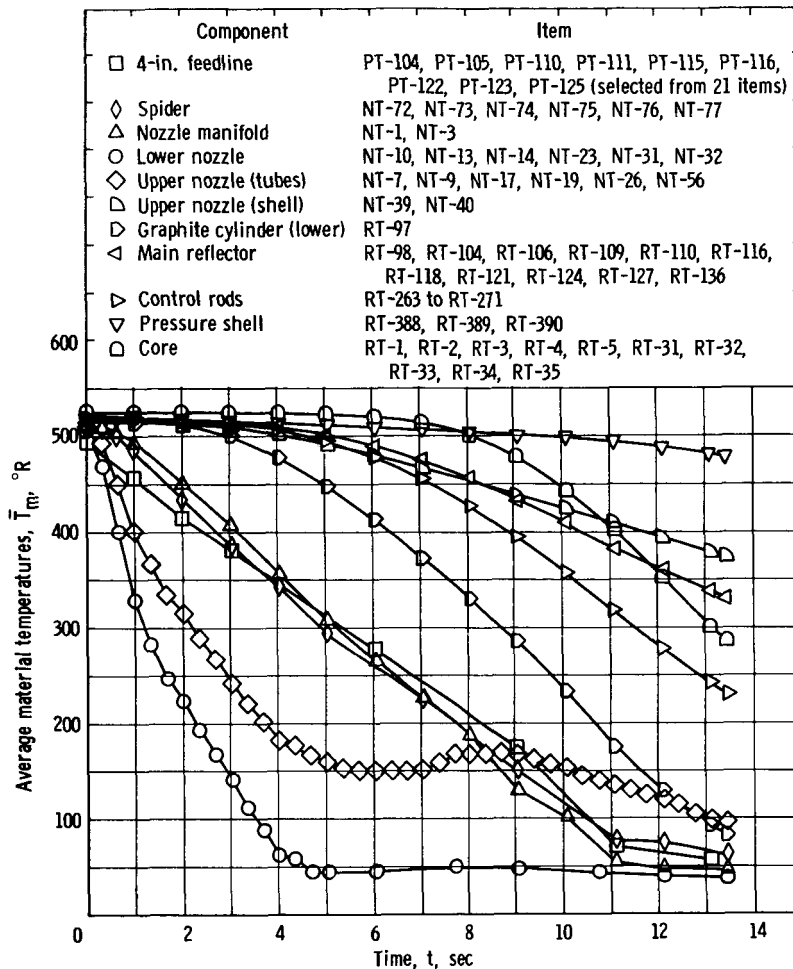


Figure 20. - Average experimental material temperatures. Run 24.

of the latent heat has been removed. Larger downstream components, however, have a relatively low heat-transfer rate near the beginning of the run, because of warm fluid temperatures, and account for most of the total heat-transfer rate near the end of the run, when fluid temperatures become low and component temperatures remain high.

The heat-transfer rate in the reflector inlet plenum $\dot{Q}_{m, LM}$ was based on the temperature-time history of item RT-390 located near the reflector inlet. (Data from later runs not reported herein confirmed that the temperature of the reflector inlet material was well represented by RT-390.) An additional problem was encountered in the reflector inlet plenum because of the presence of the reflector support bracket (shown in fig. 13, p. 23) that divides the flow between the inner and outer reflectors. No data were available to determine accurately the percentage of total flow that was diverted to the inner reflector.

Material temperature data were also incomplete for the dome region (reflector outlet to core inlet). The heat transferred from the metal parts to the fluid in the dome region

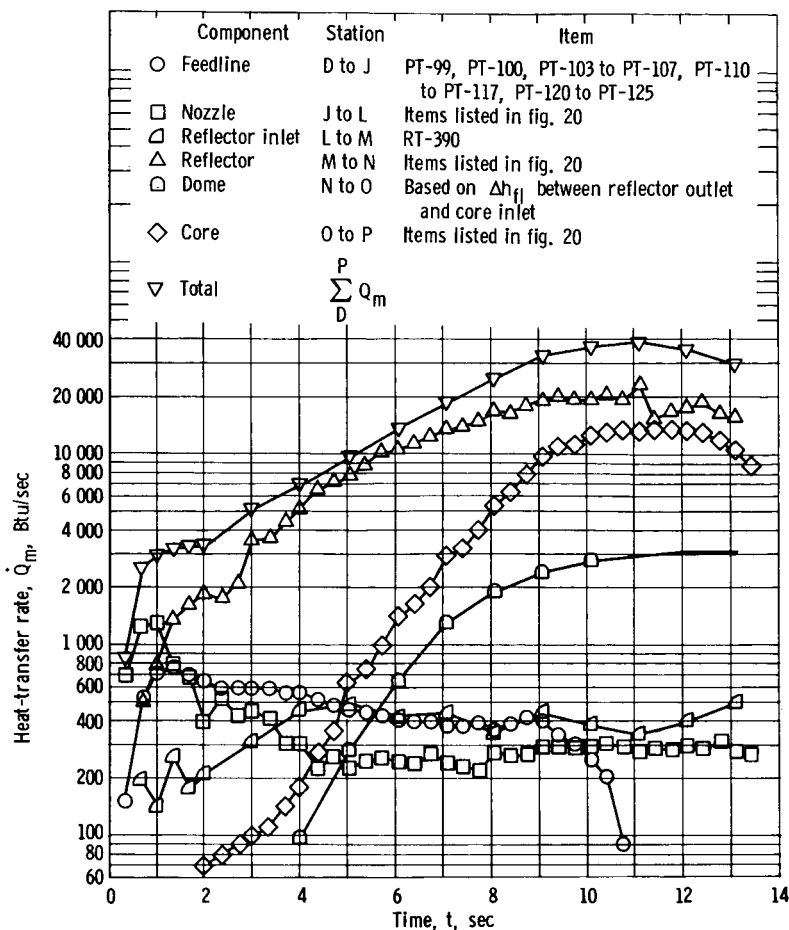


Figure 21. - Rate of heat transfer from system and components. Run 24.

$\dot{Q}_{m, NO}$ was obtained from the enthalpy rise through the region based on pressure and temperature data obtained at the reflector outlet and core inlet stations and the flow rate leaving the system ($\dot{Q}_{m, NO} = \Delta h_{NO} \dot{W}_P$). After 10 seconds, the temperature maldistribution was so great that the average temperatures were inaccurate and the curve was extrapolated, as shown in figure 21.

Calculated Results

Results of the analysis for determining the fluid properties and flow rate of the hydrogen at the various stations in the system for run 24 are presented in figures 22 to 27. The unsteady operating conditions in the first 2 seconds of the run affect all the calculated results, although the effect on enthalpy (fig. 22) and fluid temperature (fig. 23) is more pronounced.

The time of arrival of two-phase flow (indicated by the saturated gas symbols) and

the time of arrival of subcooled liquid (indicated by the saturated liquid symbols) are shown for the various stations in the system (figs. 22 to 24 and 26). For example, liquid hydrogen first arrived at station E at approximately 0.2 second, and after 3.7 seconds the fluid was subcooled. The arrival of liquid hydrogen at a station does not necessarily mean that the feedline was completely cooled. After 3.7 seconds, when heat is being transferred from the walls of the feedline to the fluid, the heat is being absorbed by the fluid, reducing the amount of subcooling.

Enthalpy. - The effect of heat transfer and flow storage on fluid enthalpy is shown in figure 22. The enthalpy of the fluid (subcooled) entering the system is the lowest curve in the figure. After 3.7 seconds, heat is still being added to the fluid between stations D and E since the enthalpy at station E is higher than at the main valve. At 10 seconds, the heat transfer is reduced to nearly zero (table IV) and the wall of the feedline in this volume increment is completely cooled. The same phenomenon is shown for other stations in the system. At 12 seconds, most of the latent heat in the system components from the inlet, station D, to the nozzle coolant tubes throat, station K, has been removed (also shown in fig. 20).

Figure 22 indicates that the duration of two-phase flow at any station between the main valve and the reflector for run 24 was about 4 seconds (time between saturated gas and saturated liquid symbols). The length of the two-phase region for this run was about

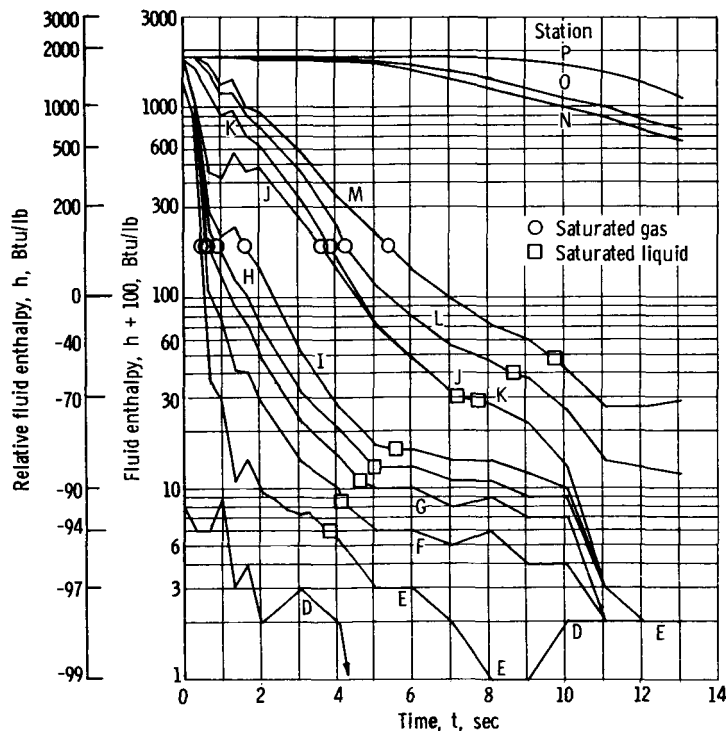


Figure 22. - Calculated fluid enthalpy at various system stations. Run 24.

[REDACTED]

20 feet at any particular time early in the run. At about 3.5 seconds, for example, the two-phase region extended from station E to station J. The duration of two-phase flow was longer and the length shorter in the larger downstream components such as the reflector. The time and space of two-phase flow vary with different flow-rate ramps and were not always uniform at all station and times.

Fluid temperature and density. - The fluid temperatures and densities presented in figures 23 and 24 were based on the calculated enthalpy, shown in figure 22, and experimental pressures at the various stations. During the periods when hydrogen density is changing rapidly, $[(\Delta\rho/\Delta t) > 2 \text{ lb}/(\text{cu ft})(\text{sec})]$ as shown in figure 24, analysis of the data is difficult due to the sensitivity of the density to small enthalpy changes. Small perturbations in heat transfer or pressure in this two-phase-flow region caused instabilities in the calculations for flow rate (eq. (7)), as was discussed in the analysis section.

Not only are the gradients steep in time, but also in space (length), as shown in figure 25 where the density profile along the length is presented at several times during run 24. Early in the run ($t < 4 \text{ sec}$) the gradient is steep near the inlet to the system between stations D and E. Later the steep gradient moves downstream and is between stations I and J at 6 seconds. When the gradient moves to the reflector ($t \geq 10 \text{ sec}$), the reflector inlet fluid is subcooled liquid and the outlet fluid is superheated gas (fig. 22).

Flow rate. - The flow rates at the various stations in run 24 are presented in figure 26. The flow rate for a particular station was assumed to be the flow rate leaving the system until the time a saturated gas condition was reached. At this point, two-phase fluid arrives at the station, and the flow rate varies with time according to the interpolation method described in the Calculation Procedure section until two-phase fluid has passed the station. At all later times in the run, the flow at that particular station was assumed to be the flow rate entering the system.

The difference between the flow rates entering and leaving the system (flow storage) was greatest in the first 8 seconds of run 24 (fig. 14). During this time, as shown in figure 26, most of the storage occurred in the feedline, that is, between the main valve and station J.

In general the flow rates at the various stations determined from the interpolation solution increased gradually with time in a consistent manner, as shown in figure 26. The flow-rate gradient in space, however, was relatively steep in the first few seconds of the run, as shown in figure 27, due to the steep density gradients previously discussed (figs. 24 and 25). The flow-rate gradients also moved downstream with increasing time in a manner similar to the steep density gradients.

The flow-rate results for runs 11, 19, 20, and 24 are presented in figure 28, where the flow rates at major stations (J, L, and P) are presented as percentages of the flow entering the system. The main difference among runs 11, 19, and 20 (figs. 28(a) to (c)) is the tank pressure that establishes the flow characteristics early in the run. All three

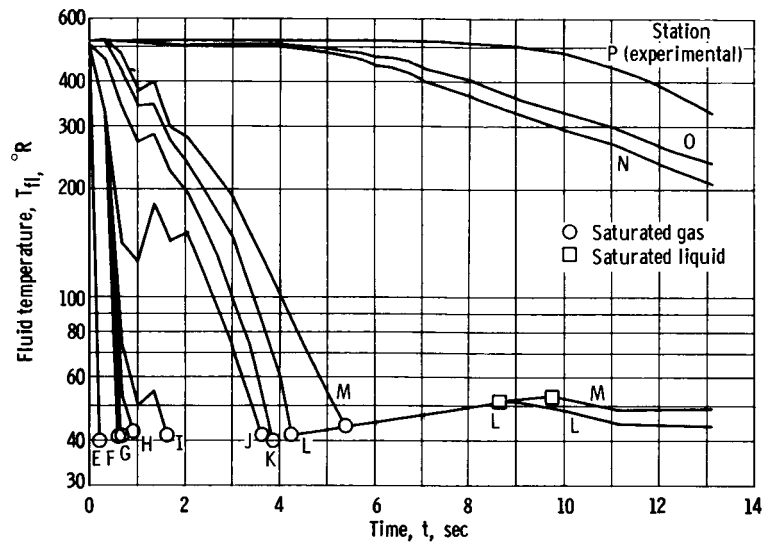


Figure 23. - Calculated fluid temperatures at various system stations. Run 24.

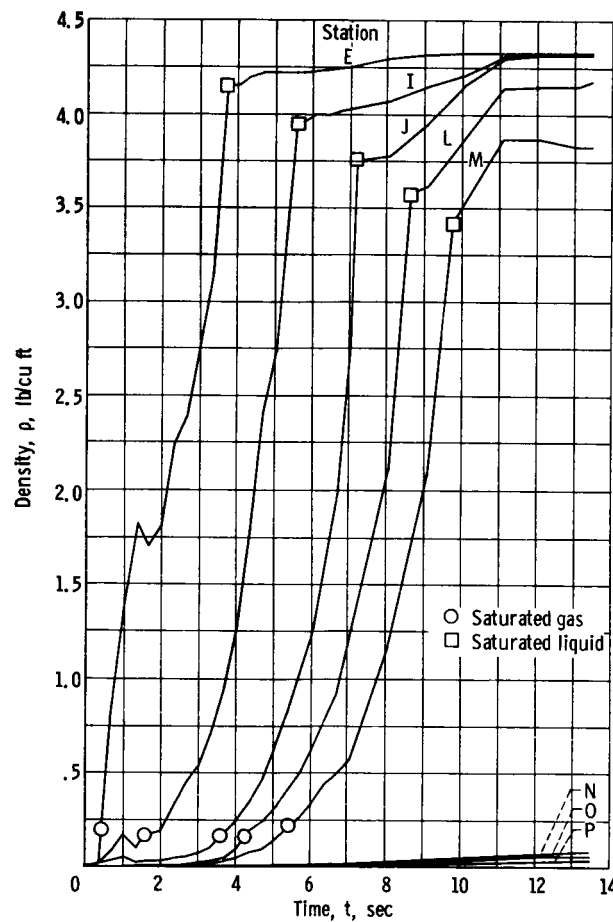


Figure 24. - Calculated hydrogen density at major system stations. Run 24.

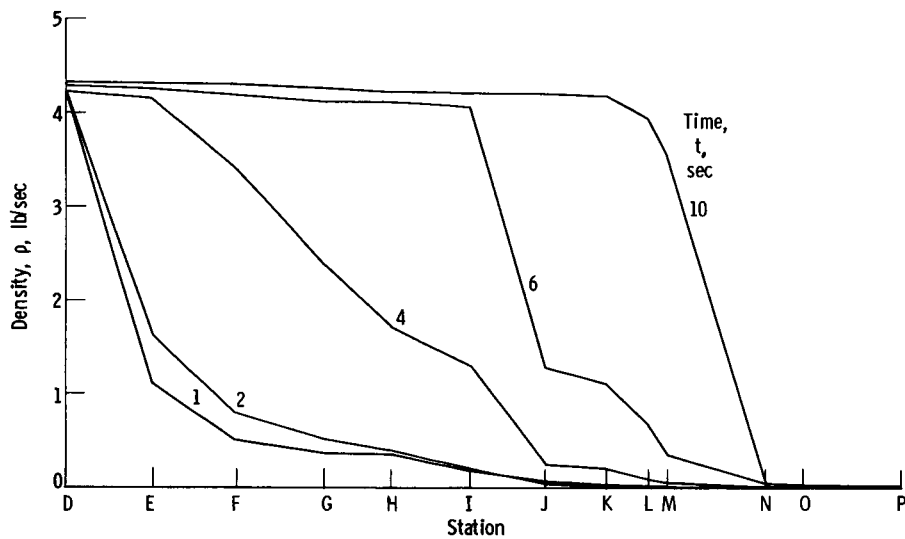


Figure 25. - Hydrogen density profile in system at several times. Run 24.

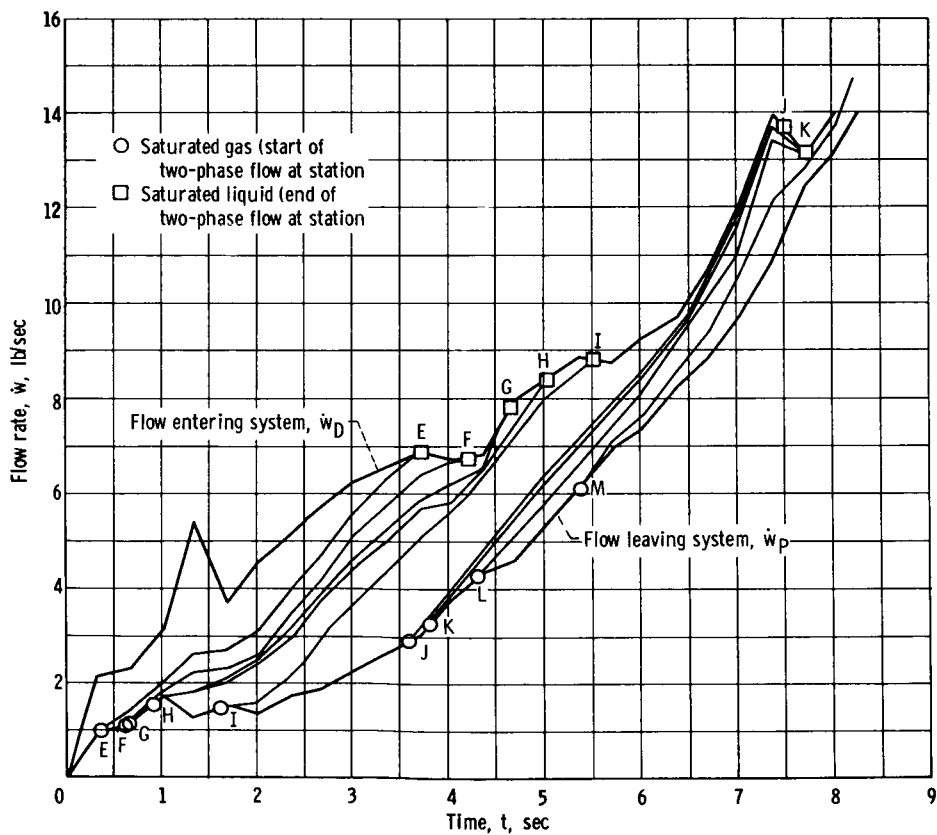


Figure 26. - Flow rate at various system stations. Run 24.

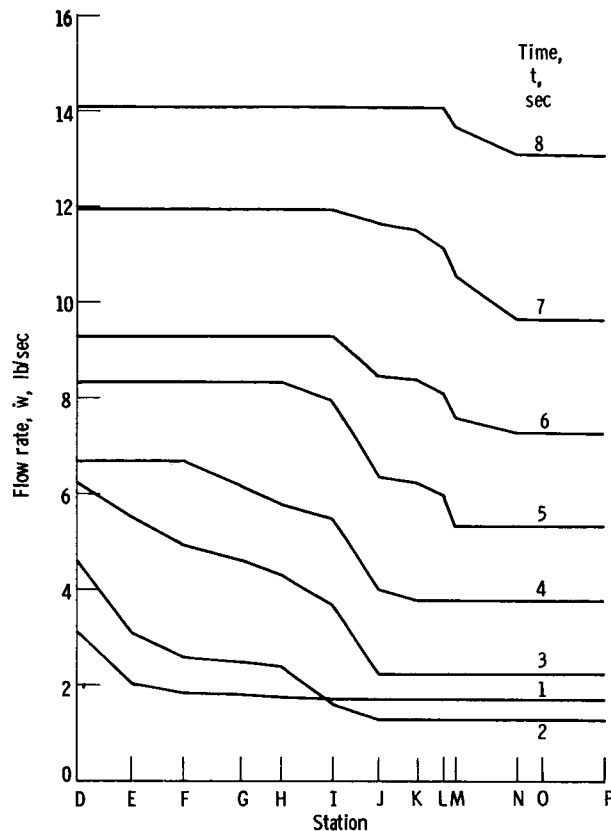


Figure 27. - Flow-rate profile in system at several times.
Run 24.

of these runs had a turbopump-control-valve delay time (6 to 10 sec). Run 24 (fig. 28(d)) had a minimal turbopump-control-valve delay time that is included for comparison.

As much as 70 percent of the flow entering the system is stored in the system in the first 3 seconds of the runs. The percentage stored then decreases as the run proceeds. The flow storage is greater in amount and duration at low tank pressures than at high tank pressures. At 50 pounds per square inch tank pressure (fig. 28(a)), for example, the flow leaving the system was generally 95 percent of the flow entering the system after about 14 seconds, whereas at 25 pounds per square inch tank pressure (fig. 28(c)) it took about 27 seconds before the flow leaving the system was generally above 95 percent of the entering flow.

The time history of flow storage at the intermediate stations (J and L) shows that most of the storage occurs in the inlet feedline during the early part of the runs as indicated by the flow at these stations being about the same as the flow leaving the system at station P. (The curve for station L in fig. 28(c) was omitted for clarity since it is located between the J and P curves.)

Even though larger fluid volumes are present downstream of the nozzle coolant tubes

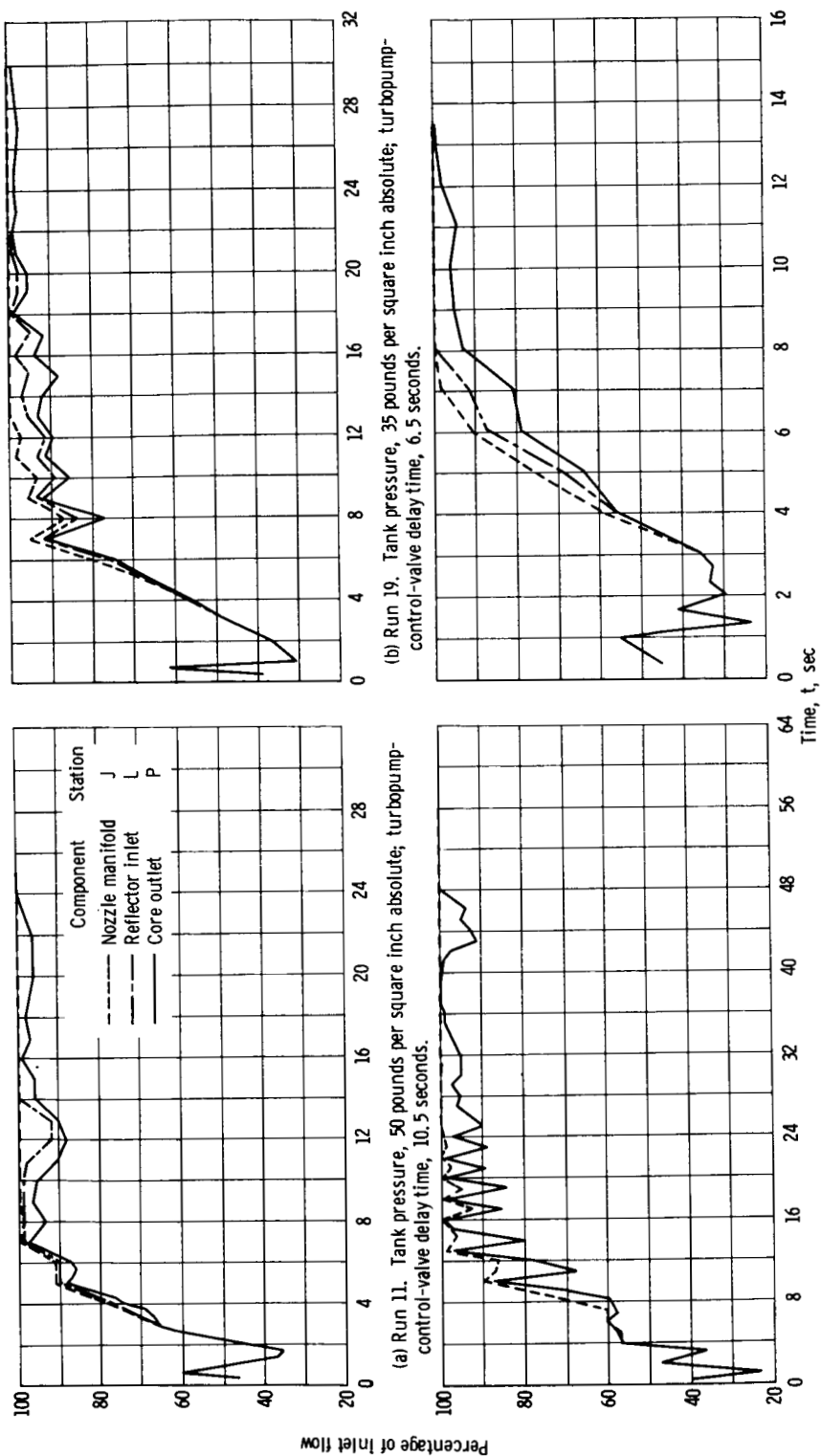


Figure 28. - Percentage of inlet flow rate at major system stations showing flow storage.

[REDACTED]

throat, flow storage is low (less than 10 percent of inlet flow) because of low hydrogen densities (fig. 29).

Flow storage in run 24 (tank pressure of 35 psia, fig. 28(d)) was about the same as for run 11 (50 psia tank pressure, fig 28(a)). The effect of minimal turbopump-control-valve delay time on flow storage at the lower tank pressure was therefore equivalent to using a higher tank pressure and about 10 seconds of turbine-power control-valve delay during the initial chilldown.

Mass balance. - The mass of hydrogen stored in each of the major components of the system was calculated by using equation (19). The results are presented in figure 30. The feedline, nozzle tubes, and reflector inlet plenum contain the greatest amount of hydrogen. Only a small mass existed in the reflector, the dome, and the core. The low values of mass in these larger components were due to the hydrogen being in the gas phase. Thus, the assumption made in the two-phase analysis that no storage occurs in the gas phase appears to be reasonable.

The total calculated mass stored in the system by the end of run 24 was about 23 pounds. The maximum liquid-hydrogen mass that could be stored in the whole system was about 120 pounds; thus, only 19 percent of the system was filled with liquid by the end of the run.

As a check on the accuracy of the interpolation solution for calculating the densities used in the stored mass equation, the sum of the mass stored in all the components should equal the difference in integrated flow rates entering and leaving the system (eq. (18)). The results of these calculations are shown in figure 31. The mass balance shows an unbalance that accumulated to about 4 pounds of hydrogen in the first 3 seconds of the run and then remained nearly constant for the remainder of the run. The stored mass based

on calculated densities $\sum_D^P M_{st}$ was lower than that determined from the integrated flows; thus, 4 pounds of stored hydrogen are not accounted for in the calculated values. Inspection of figure 26 also reveals that the mass stored between stations D and E (represented by the area between \dot{w}_D and \dot{w}_E curves) and also between stations I and J is greater than was physically possible in the corresponding incremental volumes of the feedline. In the remaining incremental volumes, the calculated stored mass and physical limitations appeared to be in reasonable agreement.

Heat balance. - Transit times were calculated for each incremental volume in the system by using equation (22) and values of $\bar{\rho}$ and \bar{w} determined from the interpolation solution. The results are presented in figure 32. The maximum transit time in each increment containing two-phase or liquid hydrogen (up to station M) was about 0.2 second. The transit time was very low ($t_t < 0.02$ sec) in the large incremental volumes containing gaseous hydrogen. The total transit time for a parcel of fluid to pass through the system varied between 0.6 and 1.2 seconds, and the corresponding shift in heat-transfer rate

[REDACTED]

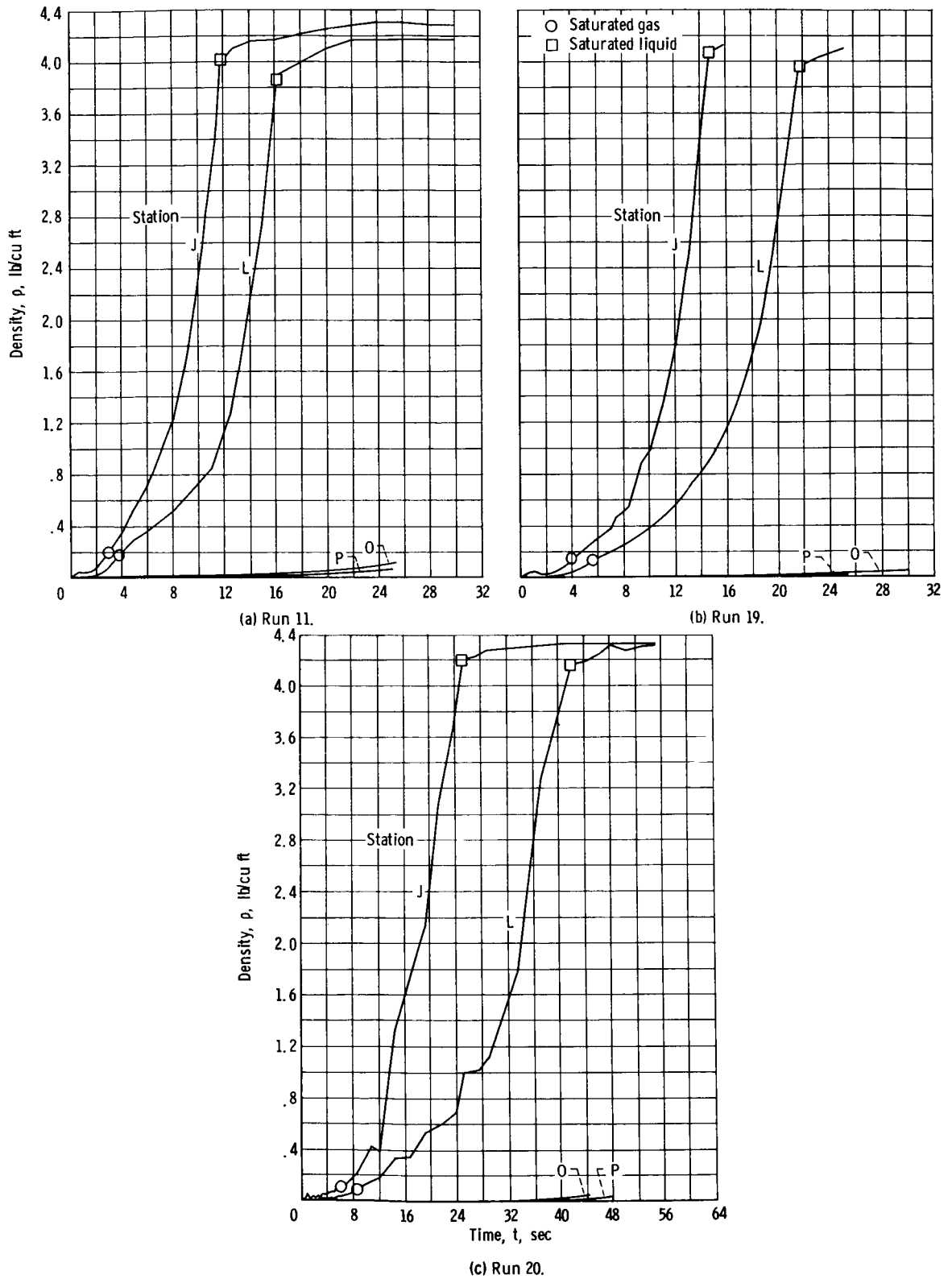


Figure 29. - Calculated hydrogen density at major system stations.

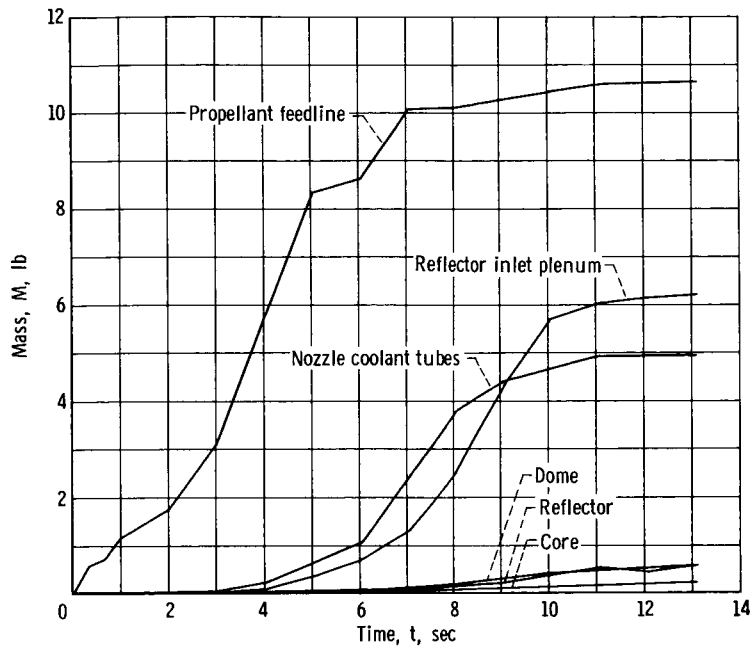


Figure 30. - Mass of hydrogen stored in major system components. Run 24.

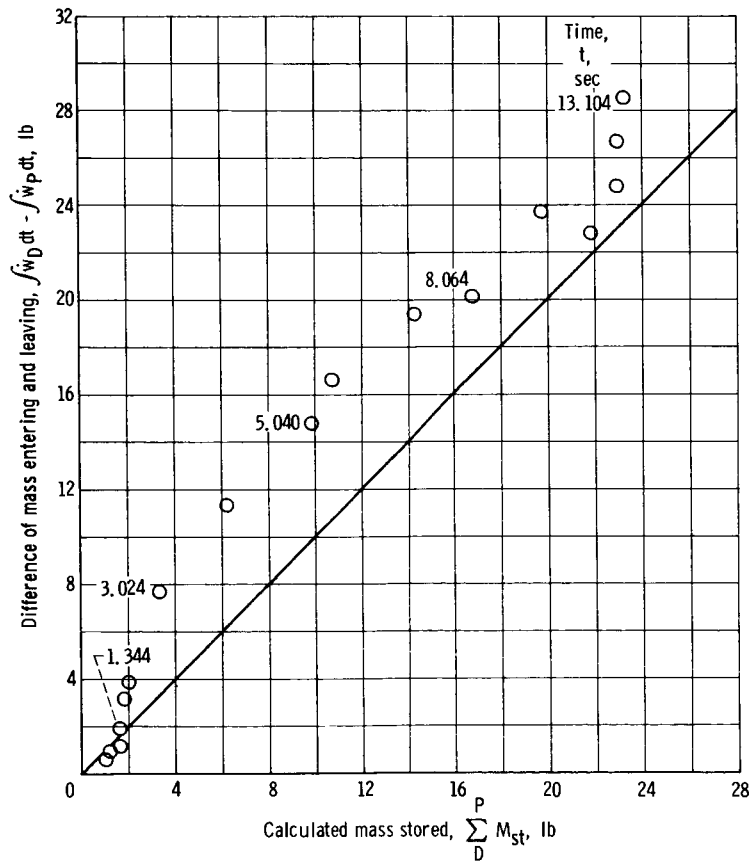


Figure 31. - Mass balance of hydrogen between main valve and exhaust nozzle. Run 24.

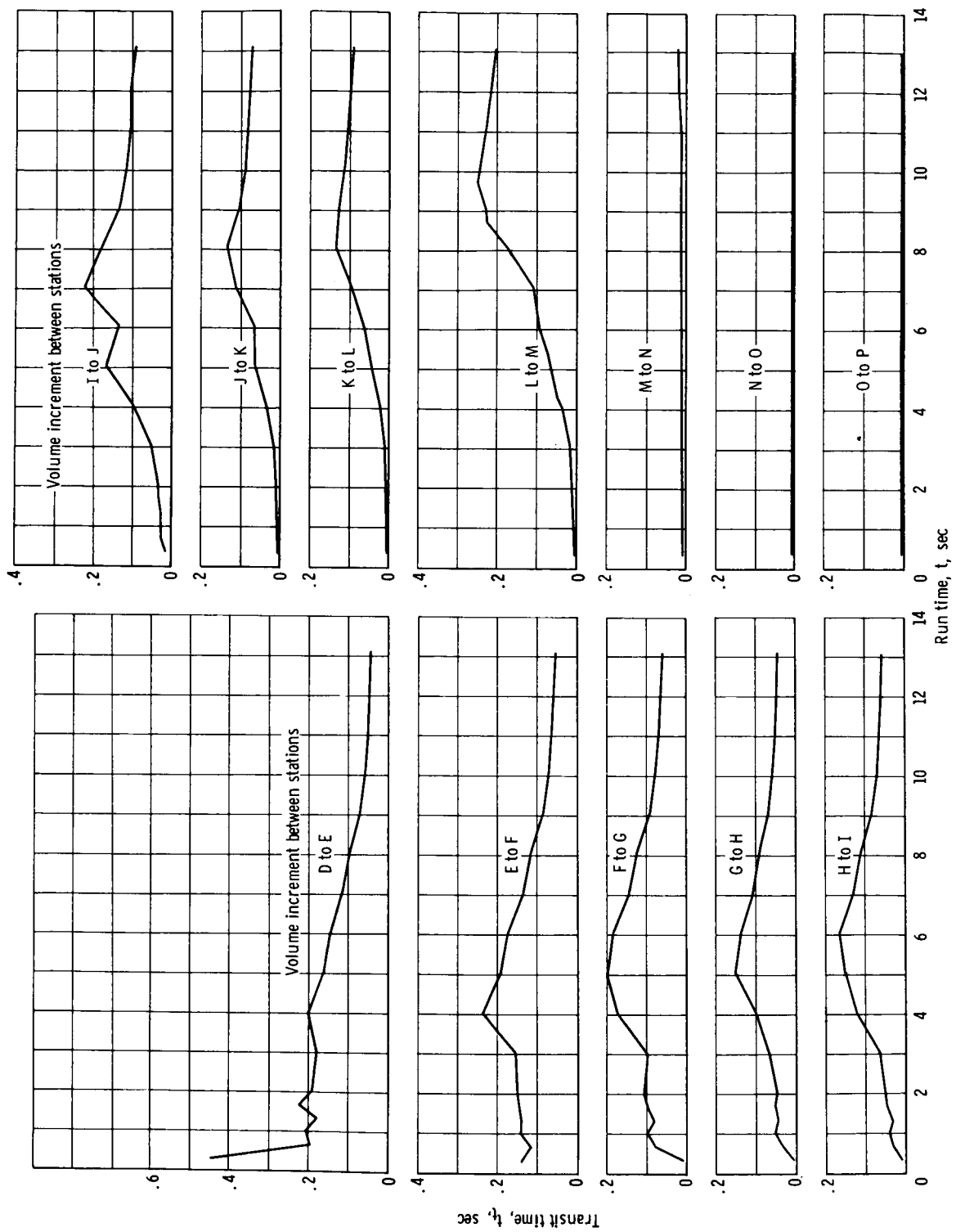


Figure 32. - Variation of fluid transit time between stations with run time. Run 24.

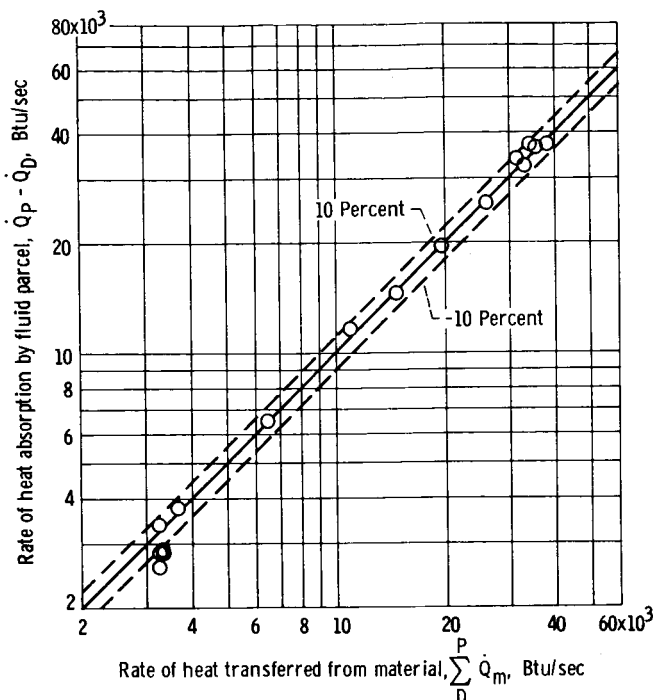


Figure 33. - Heat balance of fluid parcel between main valve and exhaust nozzle. Run 24.

(eq. (24)) was as much as 15 percent of $\dot{Q}_{fl, P} - \dot{Q}_{fl, D}$.

The result of the calculations to check the heat balance in the system is presented in figure 33, which compares the rate of heat absorbed by the fluid (eq. (24)) with the rate of heat given up by the material (eq. (25)). Agreement is within ± 10 percent for most of the data. Some of the data points at the lower end of the curve representing data obtained during the first 2 seconds of operation show a somewhat greater spread (20 percent), which is attributed to the omission of the stored energy term in the calculations and the dynamic nature of the flow during this period when experimental quantities are less accurate. The agreement shown, however, is good considering that the heat

transfer from the many large complex components is determined from relatively few temperature measurements. The effect of the transit-time correction on the heat balance was relatively small because the correction applies to both coordinates of figure 33.

Comparison of experimental and calculated flow and fluid properties. - Direct measurements of density, pressure, and fluid temperature at station I afforded a check of the calculated fluid properties using flow-rate and heat-transfer data. Comparisons of properties obtained from these measurements with calculated values from the interpolation solution for run 24 are presented in figure 34.

The experimental density data (fig. 34(a)) were about 25 percent below the calculated values. The greatest difference between the two curves occurred at 5.6 seconds where the difference is equivalent to about 50 Btu per second of heat-transfer rate. After 11 seconds, when the indicated experimental heat flow rate from the feedline was nearly zero (fig. 21) fluid-temperature measurements obtained with narrow range platinum resistance thermometers (most accurate available for steady-state readings) indicated that heat was still being added to the fluid between stations D and I. The heat rate estimated from these data was about 250 Btu per second (approximately 9 Btu/lb of hydrogen). The additional heat added to the hydrogen was probably coming from the latent heat of the insulation on the feedline (about 4500 Btu available), which was not accounted for in the calculations.

The heat flow-rate errors discussed in the previous paragraph are a small percent-

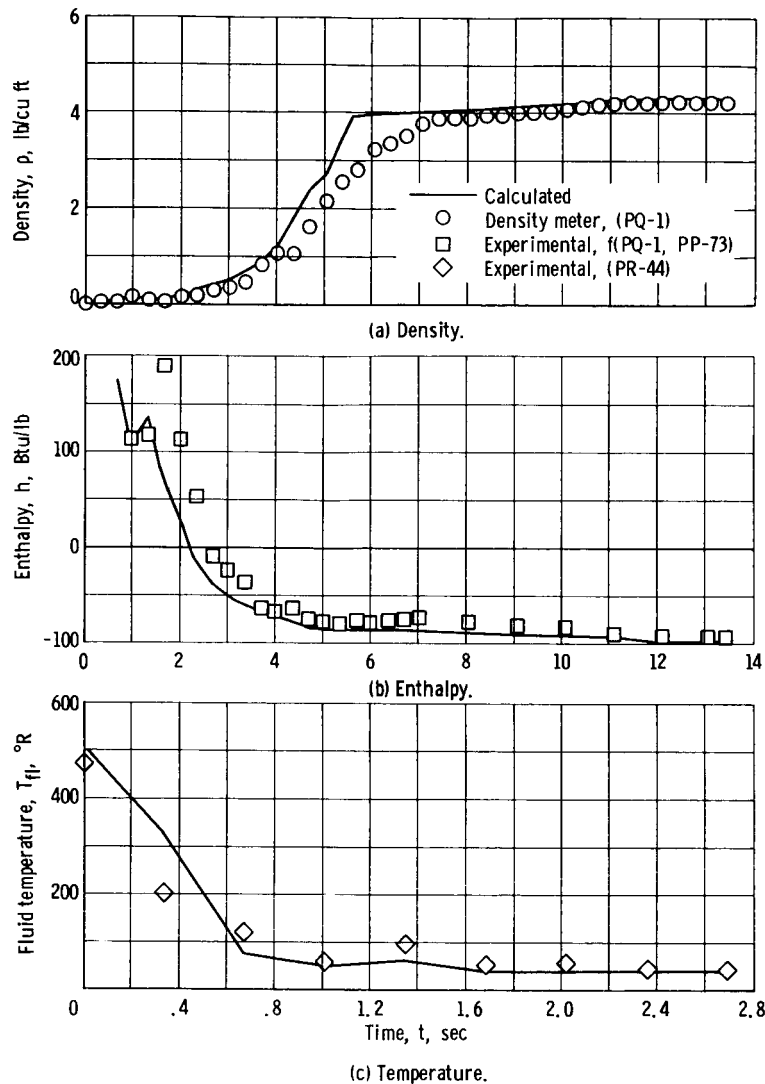


Figure 34. - Comparisons of hydrogen fluid properties obtained from experimental data with calculated values. Run 24.

age of the total heat flow-rate in the system. For component analysis, however, extraneous heat leaks should be taken into account.

Values of enthalpy below 200 Btu per pound determined from the experimental density and pressure measurements at station I are compared in figure 34(b) with the calculated values. Agreement is satisfactory considering the highly dynamic nature of the flow in the first 2 seconds and the heat added from the insulation later in the run.

Figure 34(c) presents a comparison of experimental fluid-temperature data (uncorrected for time constant) with calculated values at station I. Again agreement is good considering the nature of the flow.

~~CONFIDENTIAL~~

Although the interpolation calculation method produced results that are useful for engineering purposes, additional work may result in improved accuracy. Numerical-analysis techniques can probably be devised, for example, to overcome the stability and cumulative error problems that were encountered in the finite-difference solutions for flow rate. Much of the difficulty in these finite-difference equations even when small time and/or length increments are used is a result of the sensitivity of density to small changes in enthalpy and pressure in the low quality two-phase region. Difficulty was also encountered in calculating enthalpy because of the sensitivity of enthalpy to experimental error in heat-flow measurements.

Refinements in the interpolation solution approach may also yield improvements while retaining the simplicity of the procedure. Use of a suitable nonlinear interpolation scheme, for example, may help in achieving an improved mass balance in the system. In spite of the mass balance problem, the agreement between experimental and calculated fluid properties at station I using the linear interpolation method is encouraging. The densities measured by the calibrated density meter were probably more accurate than the calculated results.

SUMMARY OF RESULTS

Analysis of the experimental heat transfer and flow data obtained in several startup chillover transients of a full-scale nuclear rocket system simulating a flight-type configuration yielded the following principal results:

1. A simple interpolation-solution method was derived that permitted calculation of two-phase flow rate and fluid properties at various system stations using only fluid-pressure and component-material-temperature measurements and known flow conditions at the system inlet and outlet. Good agreement was obtained with direct measurement of two-phase flow density available at one station in the system.

2. Results of the analysis using the interpolation method indicate that large flow, density, and enthalpy gradients exist in both time and space in most of the components. Accurate heat transfer analyses of the components would then require that small time and length increments be used, especially in the low quality two-phase region where flow rate and density gradients were steep.

3. Detailed analysis of one run with a fast flow rate ramp indicated that two-phase flow prevailed for a duration of about 4 seconds at each station between the main valve and the reflector and existed along about 20 feet of the length of the system early in the run. Flow-rate control during this period of two-phase flow, when oscillations often occur, is important for successful startup.

4. The analysis produced flow-storage information to assist in the selection of sta-

~~CONFIDENTIAL~~

tions for measurement and control of flow rate during startup. As much as 70 percent of the flow entering the system in the first 3 seconds was stored in the system (most of it accumulated in the feedline). The length of time required for the flow rate leaving the system to equal the entering flow rate increased at lower tank pressures. For example, at a tank pressure of 50 pounds per square inch absolute, 14 seconds passed before the flow leaving the system was within 5 percent of the entering flow and at a tank pressure of 25 pounds per square inch absolute, 27 seconds were required.

Lewis Research Center,

National Aeronautics and Space Administration,

Cleveland, Ohio, September 23, 1966,

122-29-01-03-22.

~~CONFIDENTIAL~~

APPENDIX A

SYMBOLS

A	internal flow area	Subscripts:	
C_D	nozzle flow coefficient	A, B, . . . Q	stations in system
C_p	specific heat at constant pressure	bl	bleed
h	enthalpy	f	flowmeter
M	mass	fl	fluid
p	pressure	hg	hot-gas side of nozzle
\dot{Q}	heat flow rate	i	length or volume increment between any two adjacent stations
T	temperature		
t	time	in	in
t_t	transit time	int	interpolated
u	internal energy	j	any station
V	volume	m	material
v	velocity	out	out
\dot{w}	flow rate	s	static
x	distance from reference datam line	sg	saturated gas
z	distance from top of core	sl	saturated liquid
γ	specific-heat ratio	st	stored
θ	angular measurement	t	time
ρ	density	w	wall
Φ	expansion factor in nozzle flow equation	Superscript:	
		—	average value

APPENDIX B

INSTRUMENTATION AND ACCURACIES

The accuracy estimates for all measurements include errors inherent in the sensors themselves, line noise, and errors in the recording system. The errors due to line noise and the recording system were measured for each parameter before the runs and were less than 0.5 percent of full scale. Details of installation technique, problems, and accuracy of the various types of measurements are discussed in the following paragraphs.

Flow-Rate Accuracy

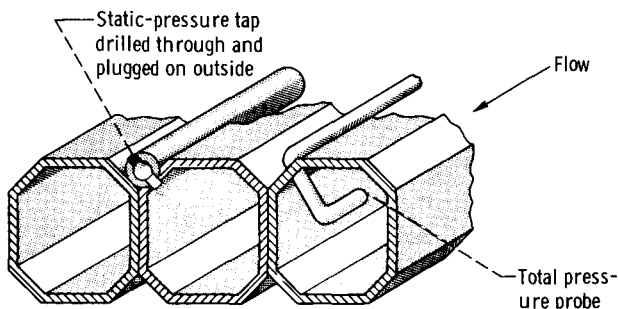
The 4-inch turbine-type flowmeter (item TF-1) was rated by the manufacturer to measure liquid-hydrogen flows from 0 to 20 pounds per second. The flowmeter was calibrated by an independent laboratory with flow rates from 0 to 14 pounds per second (maximum capacity of facility). The calibration is estimated to yield results within 2 percent. Above 14 pounds per second, comparison of flow rates determined from the rate of change of liquid level measured by a continuous capacitive type sensor (item TL-1, fig. 9) and by thermocouple point sensors (items TT-7, TT-8, and TT-9, fig. 9) indicated agreement with the turbine-type flowmeter flow rates within 10 percent.

Reference 2 discusses problems encountered in calculating flow rates from measurements obtained in the exhaust nozzle. At gas temperatures below 250° R, large maldistributions in temperatures existed, and flow coefficients for the nozzle were also not available. No nozzle flow accuracy estimate was therefore attempted.

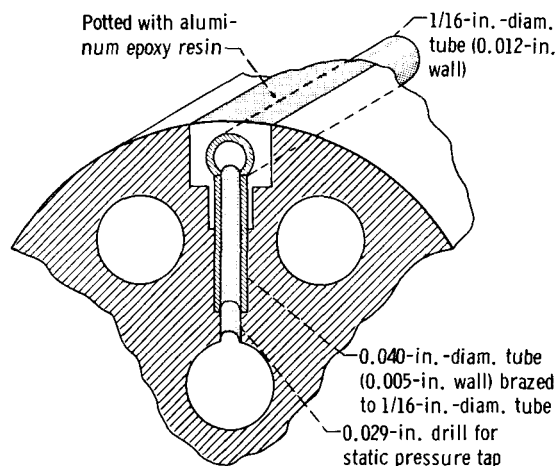
Pressure Measurement

Typical installation techniques for pressure sensing points are shown in figure 35. The technique for pressure measurement in thin wall nozzle tubes and in graphite parts is presented in figures 35(a) and (b), respectively. Many of the sensing points in the reactor and nozzle are such that the transducer cannot be located at the sensing point. The pressure is therefore transmitted through long, small-diameter (1/16 in.) tubing to the transducer, which is mounted outside of the pressure vessel (fig. 35(c)). The frequency response in the long lines was estimated to be greater than 10 cycles per second, and since the pressure oscillations were of low amplitude and frequency in this part of the system, no correction was deemed necessary. When the differential pressure between two sensing points was measured and two long, small-diameter tubes were required, the

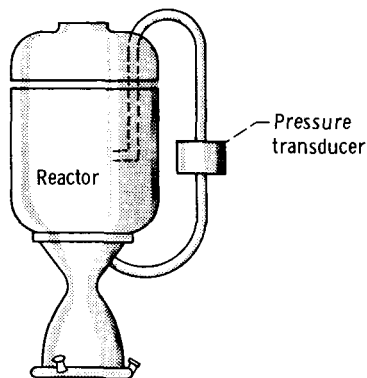
~~CONFIDENTIAL~~



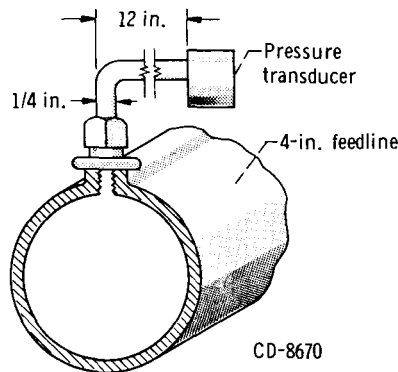
(a) Total and static-pressure measurements in nozzle coolant tubes.



(b) Static pressure measurement in fuel elements.



(c) Differential pressure measurement.



(d) Close coupled static-pressure measurement.

Figure 35. - Typical pressure measurements.

line lengths were adjusted so that equal response existed (calculated values) on both sides of the differential transducers. Measurements in the feedline and major stations in the reactor directly accessible through the pressure vessel were close coupled (fig. 35(d)).

The errors associated with the pressure transducers, approximately ± 1 percent of full scale, included a hysteresis effect, nonlinearity, and temperature shift. Corrections for zero and span settings were made in the data processing based on electrical calibrations made a few minutes before each run. Measurements made of transducer temperatures during various runs indicated the temperature effect to be completely negligible.

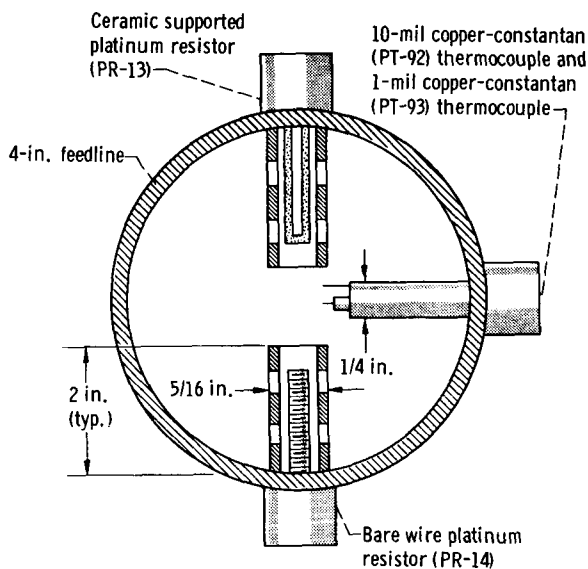
The measurement of static pressure of liquid hydrogen in system components did not pose significant problems. Total pressure measurements, however, did show a pressure oscillation that was apparently a result of the presence of a liquid-gas interface in the line connecting the sensor to the measurement point. No total pressure data

~~CONFIDENTIAL~~

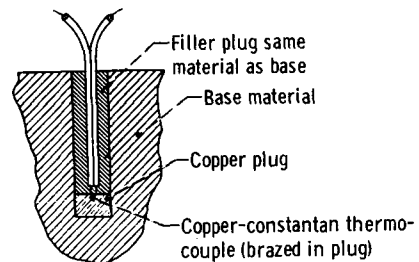
are therefore used in the data analysis. The static-pressure lines were apparently warm enough to prevent liquid from entering the tube.

Temperature Measurement

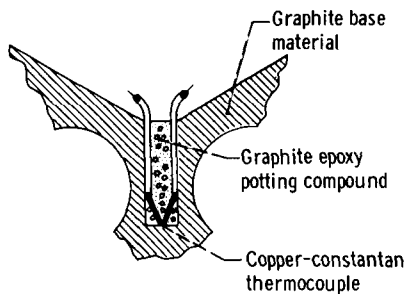
Installation of typical fluid-temperature sensors including both platinum resistance and thermocouple probes are presented in figure 36(a). All the component material temperatures were measured by using copper-constantan thermocouples. The internal material temperatures of components were measured wherever feasible by using the installation techniques shown in figure 36(b) for metal parts and in figure 36(c) for graphite parts. For thin wall locations, such as in the propellant feedline and nozzle coolant tubes, the



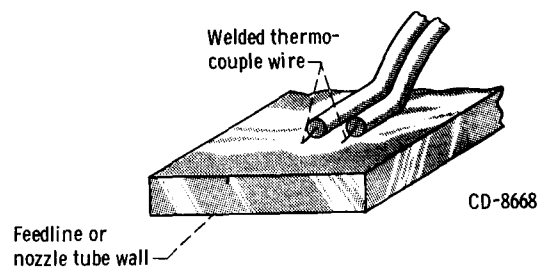
(a) Platinum resistance and thermocouple probes for fluid temperatures (station E).



(b) Thermocouple installation in metal parts.



(c) Thermocouple installation in graphite parts.



(d) Surface thermocouple installation.

Figure 36. - Typical temperature measurements.

~~CONFIDENTIAL~~

technique shown in figure 36(d) was used to obtain surface temperatures.

The calibration used for copper-constantan thermocouples conforms to the calibrations published in reference 14 to within the following limits: 200°F to $-75^{\circ}\text{F} \pm 0.75^{\circ}\text{F}$; -75°F to $-300^{\circ}\text{F} \pm 1$ percent (percent of absolute value in $^{\circ}\text{F}$). Calibration information below -300°F was obtained from an average of several thermocouples individually calibrated; no accuracy estimate has been made. In addition to the calibration errors just discussed, the curve fit of the calibration data used in the data reduction program was not exact and is estimated to contribute $\pm 1.1^{\circ}\text{F}$ errors.

The calibration for platinum resistance probes used for fluid-temperature measurements was furnished by the manufacturer. The combined overall accuracy of the measurements varies with the selected range of the bridge unit used. The accuracy varies from $\pm 9.0^{\circ}\text{R}$ at 40°R for a full range setting (20° to 540°R) to $\pm 0.4^{\circ}\text{R}$ at 40°R for a narrow range (20° to 60°R). Accuracy at temperature levels above 100°R is slightly better due to greater sensitivity.

In addition to calibration and data acquisition system errors, an appreciable error in temperature measurements can be introduced by time-constant effects during transients. Data illustrating the large magnitude (as much as 290°R) of this error during rapid transients in fluid temperatures are presented in figure 37, where the response of several temperature sensors (fig. 36(a)) to a fast ramp in temperature is shown. Data similar to those shown for several runs were used to estimate time constants of the sensors. The time constant of 1-mil thermocouples was of the order of 0.02 second, and the ceramic-supported platinum-resistance probe had a time constant of approximately 0.25 second during the early part of the transient before the start of two-phase flow.

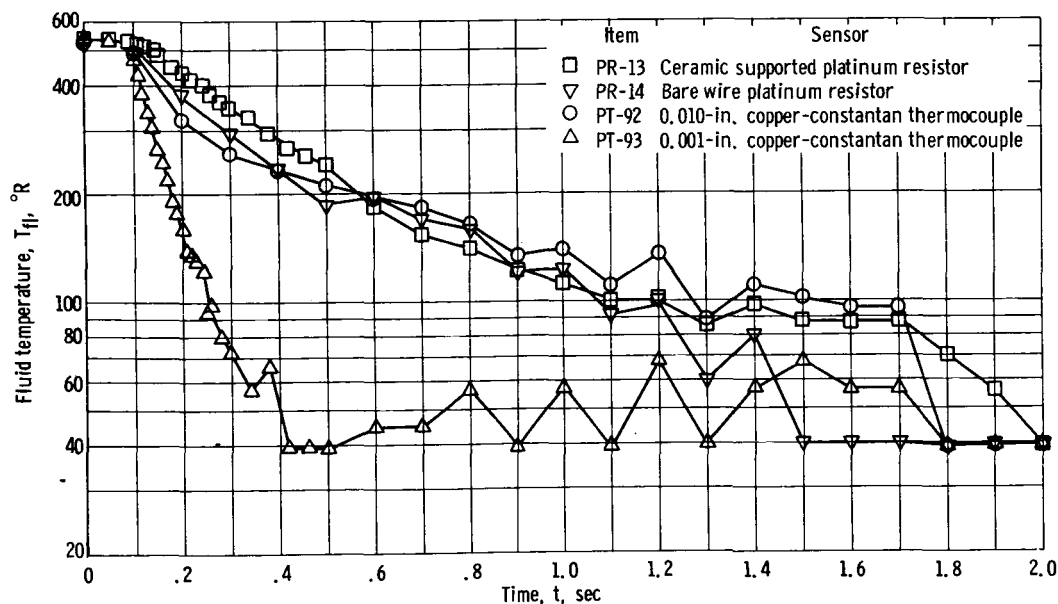


Figure 37. - Indicated fluid temperatures measured by several sensors with different time constants.

~~CONFIDENTIAL~~

After the start of two-phase flow (approximately at 0.4 sec in fig. 37), the response of the larger sensors became slower because of the lower heat-transfer rates at the surface of the sensors when low quality two-phase flow is present.

Transient errors are also possible in the measurement of material temperatures; the magnitude, however, would be much less because the rate of change of temperature is much less. Material temperature time lag is also affected by the installation method used that determines the resistance to flow of heat between the sensor and the material surrounding it and thus the time to reach steady state.

Density Measurement

A three-dimensional matrix capacitor was procured for direct measurement of quality in the propellant feedline at station I (fig. 38). The capacitance of the sensor varies with the average dielectric constant of the fluid that passes through the sensor. Use of the Clausius-Mossotti function (ref. 13), which relates density to dielectric constant, then enables determination of the density of the fluid. Voltages proportional to the capacitance itself were recorded and processed later to obtain values of density.

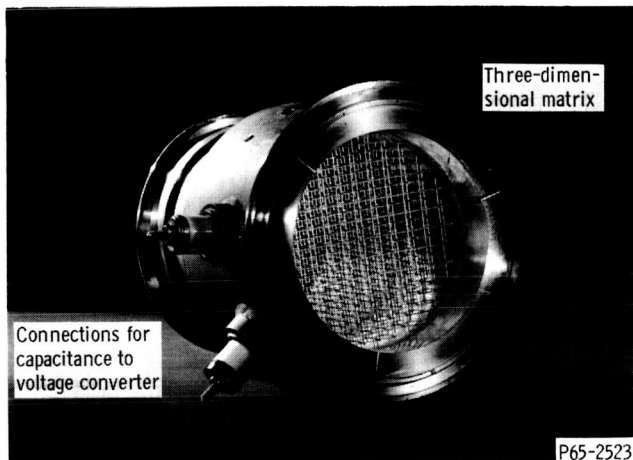


Figure 38. - Density meter sensor (PQ-1).


The density meter was calibrated during the processing of the output signal by setting the density at the time when the signal was at a minimum equal to zero (warm gas condition) and setting

the density equal to the density of subcooled liquid calculated from pressure and temperature data near the end of the run. Thus, values of the zero and span capacitances that would minimize the effects of any stray capacitances, temperature shift in the calibration, and signal drifts were established for each run.



REFERENCES

1. Turney, George E.; and Cox, Eileen C.: Cooldown Characteristics of Regenerative Nozzle used in Full-Scale, Cold-Flow, Nuclear Rocket Test Facility. NASA TN D-3931, 1967.
2. Clark, John S.: Analytical and Experimental Study of Startup Characteristics of a Full-Scale Unfueled Nuclear-Rocket-Core Assembly. NASA TM X-1231, 1966.
3. Burke, J. C.; Byrnes, W. R.; Post, A. H.; and Ruccia, F. E.: Pressurized Cool-down of Cryogenic Transfer Lines. Vol. 4, Advances in Cryogenic Engineering, K. D. Timmerhaus, ed., Plenum Press, 1960, pp. 378-394.
4. Anon: Nuclear Engine Transient Analysis Programs. Vols. I and II, Rep. No. RN-DR-0068, Aerojet General Corp., REON, Oct. 1965.
5. Ellerbrock, Herman H.; Livingood, John N. B.; and Straight, David M.: Fluid-Flow and Heat-Transfer Problems in Nuclear Rockets. Proceedings of the NASA-University Conference on the Science and Technology of Space Exploration, vol. 2, NASA SP-11, 1962, pp. 87-116. (Also available as NASA SP-20.)
6. Straight, David M.: Heat-Transfer and Flow Data with Cryogenic Hydrogen for Nuclear Rocket System Design. The Role Cryogenics is Playing in Expanding Mechanical Engineering, V. J. Johnson, ed., Natl. Bur. Std., 1963, pp. 67-84.
7. Graham, Robert W.; Hendricks, Robert C.; and Ehlers, Robert C.: Analytical and Experimental Study of Pool Heating of Liquid Hydrogen over a Range of Accelerations. NASA TN D-1883, 1965.
8. Jarvis, Stephen, Jr.: On the Formulation and Numerical Evaluation of a Set of Two-Phase Flow Equations Modeling the Cooldown Process. Tech. Note 301, Natl. Bur. Std., Jan. 1965.
9. Lee, John F.; and Sears, Francis W.: Thermodynamics. Addison-Wesley Publ. Co., Inc., 1955.
10. Bagwell, David: TQSS - An IBM-7090 Code for Computing Transient or Steady State Temperature Distributions. Rep. No. K-1494, ORNL, Gaseous Diffusion Plant, Dec. 1, 1961.
11. Rostafinski, Wojciech; Rudey, Richard A.; Lacy, Donald D.; Lillis, Patrick R.: Performance Characteristics of an Axial-Flow Liquid-Hydrogen Pump During Startup. NASA TM X-1213, 1966.
12. Roder, Hans M.; and Goodwin, Robert D.: Provisional Thermodynamic Functions for Para-Hydrogen. Tech. Note 130, Natl. Bur. Std., Dec. 1961.

- 
13. Corruccini, R. J.: Dielectric Constant of Liquid Parahydrogen. Tech. Note 144, Natl. Bur. Std., Apr. 1962.
 14. Kindler, Herbert S.; and Owens, H. Keith, eds.: Standards and Practices for Instrumentation. Inst. Soc. Am., 1963, pp. 8-12.

[REDACTED]

"The aeronautical and space activities of the United States shall be conducted so as to contribute . . . to the expansion of human knowledge of phenomena in the atmosphere and space. The Administration shall provide for the widest practicable and appropriate dissemination of information concerning its activities and the results thereof."

—NATIONAL AERONAUTICS AND SPACE ACT OF 1958

NASA SCIENTIFIC AND TECHNICAL PUBLICATIONS

TECHNICAL REPORTS: Scientific and technical information considered important, complete, and a lasting contribution to existing knowledge.

TECHNICAL NOTES: Information less broad in scope but nevertheless of importance as a contribution to existing knowledge.

TECHNICAL MEMORANDUMS: Information receiving limited distribution because of preliminary data, security classification, or other reasons.

CONTRACTOR REPORTS: Scientific and technical information generated under a NASA contract or grant and considered an important contribution to existing knowledge.

TECHNICAL TRANSLATIONS: Information published in a foreign language considered to merit NASA distribution in English.

SPECIAL PUBLICATIONS: Information derived from or of value to NASA activities. Publications include conference proceedings, monographs, data compilations, handbooks, sourcebooks, and special bibliographies.

TECHNOLOGY UTILIZATION PUBLICATIONS: Information on technology used by NASA that may be of particular interest in commercial and other non-aerospace applications. Publications include Tech Briefs, Technology Utilization Reports and Notes, and Technology Surveys.

Details on the availability of these publications may be obtained from:

SCIENTIFIC AND TECHNICAL INFORMATION DIVISION
NATIONAL AERONAUTICS AND SPACE ADMINISTRATION

Washington, D.C. 20546

[REDACTED]